Geophysical Journal International

Geophys. J. Int. (2015) **203,** 1541–1574 doi: 10.1093/gji/ggv377
GJI Marine geosciences and applied geophysics

Efficient 3-D controlled-source electromagnetic modelling using an exponential finite-difference method

Piyoosh Jaysaval,[1] Daniil V. Shantsev[2] and Sébastien de la Kethulle de Ryhove[2]

[1]*Department of Physics, University of Oslo, P.O. Box* 1048 *Blindern,* 0316 *Oslo, Norway. E-mail: piyoosh.jaysaval@fys.uio.no*
[2]*EMGS, I&I Technology Center, P.O. Box* 2087 *Vika,* 0125 *Oslo, Norway*

Accepted 2015 September 7. Received 2015 September 7; in original form 2015 March 27

SUMMARY

We have developed an efficient numerical scheme for 3-D electromagnetic (EM) simulations using an exponential finite-difference (FD) method with non-uniform grids. The method uses the set of exponential basis functions $\{1, \exp[\pm(\nu_x x + \nu_y y + \nu_z z)]\}$, where the exponents ν_x, ν_y and ν_z must be chosen carefully depending on the simulation frequency and local node conductivity. The method achieves an approximation of the oscillatory and exponentially decaying EM fields that is better than that obtained via the low-degree polynomial fitting from standard FDs—and hence also leads to more accurate results. An important property of the exponential FD method is that it tends to the standard FD method when the exponents ν_x, ν_y and ν_z tend to zero. We applied the standard and exponential FD methods to three marine controlled-source EM modelling scenarios: deep-water, shallow-water and intermediate water depth. For the deep-water scenario, we found that the proposed exponential FD method gave two to three times more accurate results as compared to the standard FD method on the same grid. For the shallow-water and intermediate water depth scenarios, the exponential FD method improved the accuracy of the upgoing fields; it gave 2–2.5 times more accurate results for the upgoing fields than the standard FD method on the same grid. Consequently, the method can achieve the same accuracy with a coarser grid and hence is faster than the standard FD method, as demonstrated using a frequency-domain iterative solver.

Key words: Numerical solutions; Numerical approximations and analysis; Electrical properties; Electromagnetic theory; Marine electromagnetics.

INTRODUCTION

Inversion and interpretation of electromagnetic (EM) data needs a fast and accurate forward modelling scheme to calculate the EM fields in arbitrary conductivity structures. This requires solving Maxwell's equations either in the time or transform (e.g. frequency) domain. Methods for numerical modelling of EM fields include the finite-difference (FD), finite-volume (FV), finite-element (FE) and integral equation (IE) methods (see e.g. Avdeev 2005; Zhdanov 2009; Börner 2010 for details). The FD and FE methods are the most popular methods; both these methods deal directly with the partial differential equations (PDEs) that govern the physics of the EM problems. Since derivatives in PDEs require only local information, the system matrix obtained by low-order discretization of the governing frequency-domain PDEs is sparse and can be computed easily. This sparseness is vital to make the solvers—direct, iterative or hybrid—used to solve the system of linear equations fast and efficient.

In the FD method, the fields and conductivities are sampled at the nodes of a finite grid. To obtain a solution of the governing PDEs, the field derivatives are replaced by FDs. The standard FD method replaces these derivatives using truncated Taylor's series expansion of the fields with low-degree polynomials determined from the field values at a small number of neighbouring nodes. The truncation of Taylor's series is based on the basic assumption that the fields between the nodal points behave as smooth and low-degree polynomials. However, if the fields have oscillatory, exponential, hyperbolic, singular, or other non-linear behaviours then this assumption requires a relatively fine grid to obtain accurate results. An example of such fields is the solution of Maxwell's equations, which has oscillatory and exponentially decaying behaviours in the frequency domain.

Several methods have been suggested to get accurate results on coarser grids if the fields exhibit strongly non-linear behaviours. One possibility is to use optimally refined non-uniform grid with coarsening of cell sizes away from the source. An example for an EM problem can be found in Davydycheva *et al.* (2003), who use a spectrally optimal refined grid achieved through special aggressively increasing cell sizes

outside the source–receivers domain, while keeping the same standard FD operator. This approach minimizes the error locally at the receivers and optimizes the boundary conditions at infinity. A second possibility is to use a high-order FD method, which allows a more accurate approximation of the derivatives in the PDEs. However, this increases the computational cost and complicates the algorithm. Moreover, if the media parameters vary rapidly at the boundaries, the high-order FD approximations can actually increase the error (Taflove & Hagness 2005; Symes *et al*. 2008).

A third possibility is to use an optimization procedure introduced by Holberg (1987) to compute the approximation coefficients of the FD operator instead of using Taylor's series, see for example Mittet (2010) for application to an EM problem. A fourth possibility is to use non-standard FD methods that preserve the properties of the numerical solution(s) of the physical problem, see Mickens (2000, 2005), Patidar (2005) and the references therein for details. These non-standard FD methods modify the FD operator according to the behaviours of the fields. Cole & Banerjee (2003) have introduced a non-standard FD operator for time-domain Maxwell's equations in a linear conducting media having no electric or magnetic current source. To get this non-standard FD operator, they use a correction function (some complex function of cell size) in the denominator of the FD approximation of derivatives instead of using simple monomials of cell size as in the standard FD method, and determine this correction function based on the oscillatory and exponentially decaying behaviours of the EM fields. They demonstrate good improvements in the accuracy by using this non-standard FD operator.

In this paper, we present a novel approach—the exponential FD method—for 3-D EM modelling with non-uniform grids. The method modifies the FD operator according to the EM field behaviour. In this method, the fields between the nodal points are locally approximated using the set of exponential basis functions $\{1, \exp[\pm(\nu_x x + \nu_y y + \nu_z z)]\}$, where ν_x, ν_y and ν_z are complex exponents. The method follows the work done on exponential fitting of derivatives by Ixaru (1997) and Ixaru & Berghe (2004) using uniform grids and by Ray (2011) and Jaysaval (2012), respectively, for 1-D and 2-D magnetotelluric (MT) modelling using non-uniform grids. We extend the theory and application of the exponential FD method to the 3-D EM case and to non-uniform grids. The method handles better the oscillatory and exponentially decaying behaviours of the EM fields and provides more accurate results as compared to the standard FD method on the same grid. Furthermore, the exponential FD method requires unknown exponent parameters ν_x, ν_y and ν_z that need to be chosen properly in accordance with the characteristics of the fields. We choose near-optimal values of these exponents based on the simulation frequency and local node conductivity. An important property of the exponential FD method is that it tends to the standard FD method when the exponents ν_x, ν_y and ν_z tend to zero (e.g. if either frequency or conductivity tends to zero)—which enables us to say that the exponential FD method is a natural extension of the standard FD method. We restrict the FD approximations to second-order because it is the simplest to illustrate the efficiency of exponential FD method against the standard FD method. High-order approximations can be constructed using second-order approximations as a base, but this is beyond the scope of this paper.

In the next sections, we first briefly describe frequency-domain EM modelling with the standard FD method. This is followed by the theory of the exponential FD method: we derive exponential FD approximations to the second-order derivatives, and thereafter describe the selection of values for the exponents ν_x, ν_y and ν_z. We then derive expressions for the truncation errors in the standard and exponential FD methods and compare the two for the special case of a broadside electric field in a uniform homogeneous medium, having a behaviour which is typical for CSEM. We subsequently compare the efficiency of the standard and exponential FD methods for deep-water marine controlled-source electromagnetic (CSEM) models. We then move to shallow-water and intermediate water depth examples, where efficiency comparisons are first made for the total electric field and then for the upgoing component of the electric field, obtained using up-down decomposition (Amundsen *et al*. 2006; Nordskag & Amundsen 2007). The reason for this decomposition is to exclude the downgoing airwave, which has little value for CSEM applications and propagates mostly through the non-conductive air, where the accuracy of both FD methods is almost identical. Finally, we draw some concluding remarks.

FD EM MODELLING SCHEME

If the temporal dependence of EM fields is $e^{-i\omega t}$, where $i = \sqrt{-1}$, then the frequency-domain Maxwell equations are given by

$$\nabla \times \mathbf{E}(\mathbf{r}) = i\omega\mu \mathbf{H}(\mathbf{r}), \tag{1}$$

$$\nabla \times \mathbf{H}(\mathbf{r}) = \bar{\boldsymbol{\sigma}}(\mathbf{r})\mathbf{E}(\mathbf{r}) - i\omega\varepsilon \mathbf{E}(\mathbf{r}) + \mathbf{J}(\mathbf{r}), \tag{2}$$

where $\mathbf{r}$ is the position vector, $\mathbf{E}$ and $\mathbf{H}$ are, respectively, the electric and magnetic fields, $\mathbf{J}$ is the electric current source, ω is the angular frequency, and μ and ε are, respectively, the magnetic permeability and dielectric permittivity. The value of μ is assumed to be constant and equal to the free space value $\mu_0 = 4\pi \times 10^{-7}$H/m. $\bar{\boldsymbol{\sigma}}(\mathbf{r})$ is the electric conductivity tensor and can vary in all the three dimensions. In a triaxial anisotropic medium, $\bar{\boldsymbol{\sigma}}(\mathbf{r})$ takes the form

$$\bar{\boldsymbol{\sigma}}(\mathbf{r}) = \begin{bmatrix} \sigma_x(\mathbf{r}) & 0 & 0 \\ 0 & \sigma_y(\mathbf{r}) & 0 \\ 0 & 0 & \sigma_z(\mathbf{r}) \end{bmatrix}, \tag{3}$$

where σ_x and σ_y are the horizontal conductivities and σ_z represents vertical conductivity.

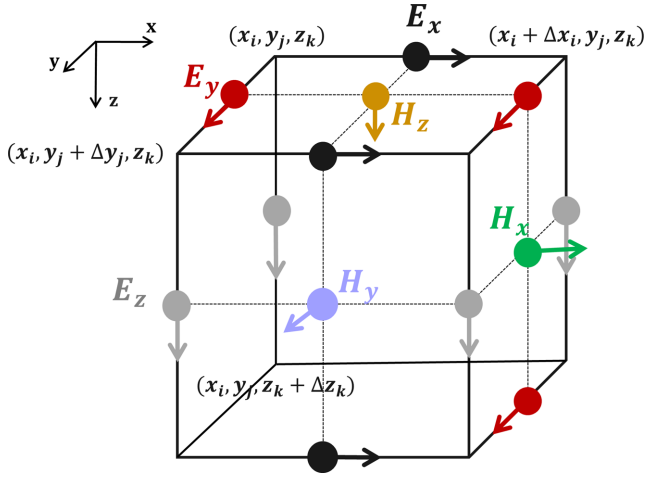

Figure 1. The staggered Yee grid used to define the positions of the electric and magnetic field nodes. The electric and magnetic field components are assigned to cell edges and faces, respectively.

By taking the curl of eq. (1) and substituting eq. (2), we obtain

$$\nabla \times \nabla \times \mathbf{E}(\mathbf{r}) - \mathrm{i}\omega\mu\tilde{\boldsymbol{\sigma}}(\mathbf{r})\mathbf{E}(\mathbf{r}) - \omega^2\mu\varepsilon\mathbf{E}(\mathbf{r}) = \mathrm{i}\omega\mu\mathbf{J}(\mathbf{r}). \tag{4}$$

Because in the CSEM method one generally uses low frequencies, in the range from 0.1 to 10 Hz, the displacement current can be neglected for typical depositional materials as $\sigma_i(\mathbf{r})/(\omega\varepsilon) \gg 1$, for $i = x, y$ and z. Therefore, eq. (4) can be rewritten as

$$\nabla \times \nabla \times \mathbf{E}(\mathbf{r}) - \mathrm{i}\omega\mu\tilde{\boldsymbol{\sigma}}(\mathbf{r})\mathbf{E}(\mathbf{r}) = \mathrm{i}\omega\mu\mathbf{J}(\mathbf{r}). \tag{5}$$

Using the definition of the curl operator in eq. (5), we obtain

$$\partial_y\partial_x E_y(\mathbf{r}) - \partial_y^2 E_x(\mathbf{r}) - \partial_z^2 E_x(\mathbf{r}) + \partial_z\partial_x E_z(\mathbf{r}) - \mathrm{i}\omega\mu\sigma_x(\mathbf{r})E_x(\mathbf{r}) = \mathrm{i}\omega\mu J_x(\mathbf{r}), \tag{6}$$

$$\partial_z\partial_y E_z(\mathbf{r}) - \partial_z^2 E_y(\mathbf{r}) - \partial_x^2 E_y(\mathbf{r}) + \partial_x\partial_y E_x(\mathbf{r}) - \mathrm{i}\omega\mu\sigma_y(\mathbf{r})E_y(\mathbf{r}) = \mathrm{i}\omega\mu J_y(\mathbf{r}), \tag{7}$$

$$\partial_x\partial_z E_x(\mathbf{r}) - \partial_x^2 E_z(\mathbf{r}) - \partial_y^2 E_z(\mathbf{r}) + \partial_y\partial_z E_y(\mathbf{r}) - \mathrm{i}\omega\mu\sigma_z(\mathbf{r})E_z(\mathbf{r}) = \mathrm{i}\omega\mu J_z(\mathbf{r}). \tag{8}$$

Eqs (6)–(8) are second-order PDEs and form the basis for our frequency-domain CSEM modelling scheme. The domain boundaries are assumed to be located sufficiently far from the transmitter for EM fields to have negligible values. Therefore, we impose Dirichlet boundary conditions by setting the electric field values to zero at all outer boundaries of the computational domain.

To obtain a solution of the Helmholtz eq. (5), PDEs (6)–(8) are discretized on a staggered Yee grid (Yee 1966) following the approach of Newman & Alumbaugh (1995). We place the electric and magnetic field components, respectively at the edges and the faces of each cell (Fig. 1). For a cell with the main node (x_i, y_j, z_k) located at the top left corner and Δx_i, Δy_j and Δz_k being, respectively, the length, width and height of this cell, the x-, y- and z-components of the electric field are located at $(x_i + \frac{\Delta x_i}{2}, y_j, z_k)$, $(x_i, y_j + \frac{\Delta y_j}{2}, z_k)$ and $(x_i, y_j, z_k + \frac{\Delta z_k}{2})$, respectively. In the same cell, the x-, y- and z-components of the magnetic field are located at $(x_i, y_j + \frac{\Delta y_j}{2}, z_k + \frac{\Delta z_k}{2})$, $(x_i + \frac{\Delta x_i}{2}, y_j, z_k + \frac{\Delta z_k}{2})$ and $(x_i + \frac{\Delta x_i}{2}, y_j + \frac{\Delta y_j}{2}, z_k)$, respectively. The discrete FD approximations to eq. (5) are given in appendix A of Newman & Alumbaugh (1995). For convenience, we list here the standard FD approximations of one second-order non-mixed derivative $\partial_y^2 E_x(\mathbf{r})$ and one second-order mixed derivative $\partial_y\partial_x E_y(\mathbf{r})$ at $(x_i + \frac{\Delta x_i}{2}, y_j, z_k)$ on the staggered grid;

$$\left.\frac{\partial^2 E_x(x, y, z)}{\partial y^2}\right|_{i+\frac{1}{2},j,k} \approx \frac{1}{\Delta y_{j-1}\Delta y_j}\left[\frac{\Delta y_{j-1}}{\Delta y_{sj}}E^x_{i+\frac{1}{2},j+1,k} - 2E^x_{i+\frac{1}{2},j,k} + \frac{\Delta y_j}{\Delta y_{sj}}E^x_{i+\frac{1}{2},j-1,k}\right], \tag{9}$$

$$\left.\frac{\partial^2 E_y(x, y, z)}{\partial y\partial x}\right|_{i+\frac{1}{2},j,k} \approx \frac{1}{\Delta x_i\Delta y_{sj}}\left[E^y_{i+1,j+\frac{1}{2},k} - E^y_{i+1,j-\frac{1}{2},k} - E^y_{i,j+\frac{1}{2},k} + E^y_{i,j-\frac{1}{2},k}\right], \tag{10}$$

where $\Delta y_{sj} = \frac{1}{2}(\Delta y_{j-1} + \Delta y_j)$. Here, the values of E_x at the nodes are indexed as $E^x_{i+\frac{1}{2},j+1,k} \equiv E_x(x_i + \frac{\Delta x_i}{2}, y_j + \Delta y_j, z_k)$ and so on.

The conductivity within each cell is assumed to be uniform. The FD discretization requires knowledge of conductivity values at each electric field node (halfway along a given cell edge). At these locations, the conductivity could be discontinuous since it often varies from cell to cell, and hence a proper conductivity averaging is required. We use the averaging method described in Taflove & Hagness (2005,

p. 492) for this purpose. For example, the x-staggered averaged conductivity at $(x_i + \frac{\Delta x_i}{2}, y_j, z_k)$ is obtained using an area-weighted averaging of the conductivity of four adjacent cells $(i, j, k-1)$, (i, j, k), $(i, j+1, k-1)$ and $(i, j+1, k)$:

$$\tilde{\sigma}^x_{i+\frac{1}{2},j,k} = \frac{\sum_{l=0}^{1}\sum_{m=-1}^{0}\Delta y_{j+l}\Delta z_{k+m}\sigma^x_{i,j+l,k+m}}{\sum_{l=0}^{1}\sum_{m=-1}^{0}\Delta y_{j+l}\Delta z_{k+m}}, \tag{11}$$

where $\sigma^x_{i,j+l,k+m}$ is the x-conductivity of the $(i, j+l, k+m)$th cell. The y- and z-staggered averaged conductivities are computed is a similar way. There are also advanced averaging formulas, for example the one presented in Davydycheva *et al*. (2003) for cases that are more complicated, for example if one wants to perform coarse grid modelling from a finely discretized model or a model that has tilted anisotropy. However, for the simple models presented in this paper both methods give identical results.

Sharp variations of conductivity also lead to discontinuities in EM fields and its derivatives, which is especially important for marine CSEM where a current source and recording stations are usually located close to the seafloor that separates conductive water and resistive formation. We use interpolation operators derived in Shantsev & Maaø (2015) that take a detailed account of these discontinuities for an arbitrary dipping angle of the seafloor.

System matrix and solution

The FD discretization of eqs (6)–(8) forms a system of linear equations

$$\mathbf{Mx} = \mathbf{s}, \tag{12}$$

where $\mathbf{M}$ is the system matrix of dimension $3N \times 3N$ for a modelling grid with $N = N_x \times N_y \times N_z$ cells, $\mathbf{x}$ is a vector of dimension $3N$ containing unknown electric field components E_x, E_y and E_z, and $\mathbf{s}$ (dimension $3N$) is the source vector resulting from the right hand side of eq. (5). The matrix $\mathbf{M}$ is a sparse complex matrix, having up to 13 non-zero elements in a row. Note that though the fields at the outer edges are zero due to Dirichlet boundary conditions, we consider the fields as unknowns at one of the two outer edges in each direction so that the total number of unknowns remains $3N$.

The matrix eq. (12) is very large for typical CSEM simulations; and involves several hundred thousand to a few million cells. Such a matrix equation can be solved by efficient direct, iterative, or hybrid solvers. Examples of modelling results obtained with a direct solver can be found in, for example Streich (2009), da Silva *et al*. (2012) and Jaysaval *et al*. (2014). All modelling results presented in this paper were obtained using an iterative solver to solve the matrix equation. This iterative solver is mainly based on the ideas presented by Mulder (2006): a complex biconjugate-gradient-type method, for example BICGStab (van der Vorst 1992), is used in combination with a multigrid preconditioner and a block Gauss–Seidel smoother. The Gauss–Seidel smoother is necessary because of the large null-space of the curl–curl operator in 3-D. Finally, after computing the electric field by solving the matrix eq. (12), Faraday's law (eq. 1) is used to calculate the magnetic field.

EXPONENTIAL FD METHOD

The standard FD approximation, based on truncated Taylor's series expansions, is good when the fields can be approximated by low-degree polynomials between the nodal points. In a situation where the fields are a weighted sum of oscillatory, exponential, or hyperbolic components, one would expect the standard FD method to be accurate only when the nodes are spaced sufficiently closely for the fields to behave as low-degree polynomials in between. The exponential FD method deals with such a class of fields by approximating them using exponential basis functions rather than simple low-degree polynomials between the nodes. Since the EM fields have oscillatory and exponentially decaying behaviours, the exponential FD method should give more accurate results than the standard FD method on a given grid.

Eqs (6)–(8) show that to define an exponential FD scheme, we need to compute exponential FD approximations to the second-order derivatives with respect to (a) one single variable [non-mixed derivatives, e.g. $\partial_y^2 E_x(\mathbf{r})$] and (b) two variables [mixed derivatives, e.g. $\partial_y\partial_x E_y(\mathbf{r})$]. In the following paragraphs we derive exponential FD approximations to $\partial_y^2 E_x(\mathbf{r})$ and $\partial_y\partial_x E_y(\mathbf{r})$, and then extend the results to obtain an exponential FD approximation to the Helmholtz equation.

Ixaru (1997) and Ixaru & Berghe (2004) have described a procedure to obtain exponential FD approximations of derivatives for uniform grid discretization, and later Ray (2011) and Jaysaval (2012) gave procedures, respectively, for 1-D and 2-D non-uniform grid discretization. We follow Jaysaval (2012) to obtain exponential FD approximations of derivatives for a 3-D non-uniform grid discretization.

Let the second-order exponential FD approximation of $\partial_y^2 E_x(\mathbf{r})$ at $(x_i + \frac{\Delta x_i}{2}, y_j, z_k)$ on the staggered grid be expressed as

$$\left.\frac{\partial^2 E_x(x,y,z)}{\partial y^2}\right|_{i+\frac{1}{2},j,k} \approx \frac{1}{\Delta y_{j-1}\Delta y_j}\left[a_1 E^x_{i+\frac{1}{2},j+1,k} + a_2 E^x_{i+\frac{1}{2},j,k} + a_3 E^x_{i+\frac{1}{2},j-1,k}\right], \tag{13}$$

with the set of unknown coefficients $\mathbf{a} \equiv [a_1, a_2, a_3]$. To obtain these coefficients, we define an operator $\mathcal{L}_{2y}[\Delta y_{j-1}, \Delta y_j, \mathbf{a}]$ as

$$\mathcal{L}_{2y}\left[\Delta y_{j-1}, \Delta y_j, \mathbf{a}\right] E_x(\mathbf{r}) = \left.\frac{\partial^2 E_x(x,y,z)}{\partial y^2}\right|_{i+\frac{1}{2},j,k} - \frac{1}{\Delta y_{j-1}\Delta y_j}\left[a_1 E^x_{i+\frac{1}{2},j+1,k} + a_2 E^x_{i+\frac{1}{2},j,k} + a_3 E^x_{i+\frac{1}{2},j-1,k}\right]. \tag{14}$$

The operator $\mathcal{L}_{2y}[\Delta y_{j-1}, \Delta y_j,\ \mathbf{a}]$ measures the misfit between the approximation in eq. (13) and the corresponding exact quantity. Our main objective is to determine a set of coefficients $\mathbf{a} \equiv [a_1, a_2, a_3]$ such that $\mathcal{L}_{2y}[\Delta y_{j-1}, \Delta y_j,\ \mathbf{a}]E_x(\mathbf{r}) = 0$; indicating that the approximation in eq. (13) would be appropriate. In exponential FD, the field $E_x(\mathbf{r})$ between the nodal points is assumed to consist of some combination of exponential basis functions $\{1, \exp[\pm(\nu_x x + \nu_y y + \nu_z z)]\}$. Values for the set of coefficients $\mathbf{a} \equiv [a_1, a_2, a_3]$ are obtained in Appendix A (eqs A1–A14) by solving $\mathcal{L}_{2y}[\Delta y_{j-1}, \Delta y_j, \mathbf{a}]1 = 0$ and $\mathcal{L}_{2y}[\Delta y_{j-1}, \Delta y_j, \mathbf{a}]\exp\{\pm(\nu_x x + \nu_y y + \nu_z z)\} = 0$, and are also reproduced here for convenience;

$$a_1 = \frac{\nu_y^2 \Delta y_{j-1} \Delta y_j}{\left[\left\{\eta_{-1}\left(\nu_y \Delta y_j\right) - 1\right\} + \left\{\eta_{-1}\left(\nu_y \Delta y_{j-1}\right) - 1\right\} \frac{\Delta y_j}{\Delta y_{j-1}} \frac{\eta_0\left(\nu_y \Delta y_j\right)}{\eta_0\left(\nu_y \Delta y_{j-1}\right)}\right]}, \tag{15}$$

$$a_3 = \frac{\Delta y_j}{\Delta y_{j-1}} \frac{\eta_0\left(\nu_y \Delta y_j\right)}{\eta_0\left(\nu_y \Delta y_{j-1}\right)} a_1, \tag{16}$$

$$a_2 = -a_1 - a_3, \tag{17}$$

where $\eta_{-1}(\nu_y \Delta y) = \frac{1}{2}[\exp(\nu_y \Delta y) + \exp(-\nu_y \Delta y)]$ and $\eta_0(\nu_y \Delta y) = \frac{1}{2\nu_y \Delta y}[\exp(\nu_y \Delta y) - \exp(-\nu_y \Delta y)]$.

Now consider the mixed derivative $\partial_y \partial_x E_y(\mathbf{r})$ at $(x_i + \frac{\Delta x_i}{2}, y_j, z_k)$ on the staggered grid

$$\left.\frac{\partial^2 E_y(x, y, z)}{\partial y \partial x}\right|_{i+\frac{1}{2}, j, k} = \frac{\partial}{\partial y}\left[\frac{\partial E_y(x, y, z)}{\partial x}\right]_{i+\frac{1}{2}, j, k} = \frac{\partial}{\partial x}\left[\frac{\partial E_y(x, y, z)}{\partial y}\right]_{i+\frac{1}{2}, j, k}. \tag{18}$$

To obtain an exponential FD approximation of $\partial_y \partial_x E_y(\mathbf{r})$, we first compute an approximation for $\frac{\partial E_y(x,y,z)}{\partial x}|_{i+\frac{1}{2}, j, k}$ followed by one for $\frac{\partial E_y(x,y,z)}{\partial y}|_{i+\frac{1}{2}, j, k}$ using exponential basis function of the form $\exp\{\pm(\nu_x x + \nu_y y + \nu_z z)\}$.
Let

$$\left.\frac{\partial E_y(x, y, z)}{\partial x}\right|_{i+\frac{1}{2}, j, k} \approx \frac{1}{\Delta x_i}\left\{b_1 E^y_{i+1, j, k} + b_2 E^y_{i, j, k}\right\}, \tag{19}$$

and

$$\left.\frac{\partial E_y(x, y, z)}{\partial y}\right|_{i+\frac{1}{2}, j, k} \approx \frac{1}{\Delta y_{sj}}\left\{c_1 E^y_{i+\frac{1}{2}, j+\frac{1}{2}, k} + c_2 E^y_{i+\frac{1}{2}, j-\frac{1}{2}, k}\right\}, \tag{20}$$

with the set of unknown coefficients $\mathbf{b} \equiv [b_1, b_2]$ and $\mathbf{c} \equiv [c_1, c_2]$. To obtain these coefficients, we define operators $\mathcal{L}_{1x}[\Delta x_i, \mathbf{b}]$ and $\mathcal{L}_{1y}[\Delta y_{j-1}, \Delta y_j, \mathbf{c}]$ as

$$\mathcal{L}_{1x}\left[\Delta x_i, \mathbf{b}\right] E_y(\mathbf{r}) = \left.\frac{\partial E_y(x, y, z)}{\partial x}\right|_{i+\frac{1}{2}, j, k} - \frac{1}{\Delta x_i}\left\{b_1 E^y_{i+1, j, k} + b_2 E^y_{i, j, k}\right\}, \tag{21}$$

and

$$\mathcal{L}_{1y}\left[\Delta y_{j-1}, \Delta y_j, \mathbf{c}\right] E_y(\mathbf{r}) = \left.\frac{\partial E_y(x, y, z)}{\partial y}\right|_{i+\frac{1}{2}, j, k} - \frac{1}{\Delta y_{sj}}\left\{c_1 E^y_{i+\frac{1}{2}, j+\frac{1}{2}, k} + c_2 E^y_{i+\frac{1}{2}, j-\frac{1}{2}, k}\right\}. \tag{22}$$

Values for the coefficients $\mathbf{b} \equiv [b_1, b_2]$ and $\mathbf{c} \equiv [c_1, c_2]$ are determined in Appendix A (eqs A15–A39) by solving $\mathcal{L}_{1x}[\Delta x_i, \mathbf{b}]\exp\{\pm(\nu_x x + \nu_y y + \nu_z z)\} = 0$ and $\mathcal{L}_{1y}[\Delta y_{j-1}, \Delta y_j, \mathbf{c}]\exp\{\pm(\nu_x x + \nu_y y + \nu_z z)\} = 0$, and are also reproduced here for convenience;

$$b_1 = -b_2 = \frac{1}{\eta_0\left(\nu_x \frac{\Delta x_i}{2}\right)}, \tag{23}$$

and

$$c_1 = \frac{2\Delta y_{sj}}{\left[\Delta y_j \eta_0\left(\nu_y \frac{\Delta y_j}{2}\right) + \Delta y_{j-1} \eta_0\left(\nu_y \frac{\Delta y_{j-1}}{2}\right) \frac{\eta_{-1}\left(\nu_y \frac{\Delta y_j}{2}\right)}{\eta_{-1}\left(\nu_y \frac{\Delta y_{j-1}}{2}\right)}\right]}, \tag{24}$$

$$c_2 = -\frac{\eta_{-1}\left(\nu_y \frac{\Delta y_j}{2}\right)}{\eta_{-1}\left(\nu_y \frac{\Delta y_{j-1}}{2}\right)} c_1. \tag{25}$$

Therefore,

$$\left.\frac{\partial^2 E_y(x, y, z)}{\partial y \partial x}\right|_{i+\frac{1}{2}, j, k} = \frac{\partial}{\partial y}\left[\frac{\partial E_y(x, y, z)}{\partial x}\right]_{i+\frac{1}{2}, j, k} \tag{26}$$

$$\approx \frac{\partial}{\partial y}\left[\frac{1}{\Delta x_i}\left\{b_1 E^y_{i+1,j,k} + b_2 E^y_{i,j,k}\right\}\right] \tag{27}$$

$$\approx \frac{1}{\Delta x_i}\left[b_1\left\{\frac{c_1 E^y_{i+1,j+\frac{1}{2},k} + c_2 E^y_{i+1,j-\frac{1}{2},k}}{\Delta y_{sj}}\right\} + b_2\left\{\frac{c_1 E^y_{i,j+\frac{1}{2},k} + c_2 E^y_{i,j-\frac{1}{2},k}}{\Delta y_{sj}}\right\}\right] \tag{28}$$

$$\approx \frac{1}{\Delta x_i \Delta y_{sj}}\left[b_1 c_1 E^y_{i+1,j+\frac{1}{2},k} + b_1 c_2 E^y_{i+1,j-\frac{1}{2},k} + b_2 c_1 E^y_{i,j+\frac{1}{2},k} + b_2 c_2 E^y_{i,j-\frac{1}{2},k}\right]. \tag{29}$$

We similarly compute exponential FD approximations for all the remaining second-order derivatives in the PDEs (6)–(8). An important property of the exponential FD approximation is that in the limiting case when the exponents v_x, v_y and v_z tend to zero (e.g. if either frequency or conductivity tends to zero), it tends to the standard FD approximation. This is proved in Appendix B. This fact allows us to say that the exponential FD approximation represents a natural extension of the low-degree polynomial-fitting based standard FD approximation.

Choice of exponents

A significant point of discussion in the development of the exponential FD method is the choice of the unknown exponents v_x, v_y and v_z in the basis functions $\exp\{\pm(v_x x + v_y y + v_z z)\}$. It is reasonable to expect that the best results will be obtained if the values of the exponents are chosen in accordance with the characteristics of the EM fields. Solution of the Maxwell's equations for a plane wave in a conducting medium is described by the factor e^{ikr}, where r is a distance and $k = (1+\mathrm{i})\sqrt{\mu\omega\sigma/2}$ is the wavenumber. For a more complicated case, for example a dipole source as in CSEM, the EM fields are proportional to e^{ikr} with additional rational expression weights (Ward & Hohmann 1988). In CSEM, for most relevant values of r, the factor e^{ikr} dominates the spatial dependence. This leads us to the following choice of the values of the exponents depending on the simulation frequency and conductivity of each node: $v_x = v_y = v_z = \pm(1-\mathrm{i})\sqrt{\mu\omega\sigma_x/2}$ for all derivatives in the x-projection (6), $v_x = v_y = v_z = \pm(1-\mathrm{i})\sqrt{\mu\omega\sigma_y/2}$ for all derivatives in the y-projection (7) and $v_x = v_y = v_z = \pm(1-\mathrm{i})\sqrt{\mu\omega\sigma_z/2}$ for all derivatives in the z-projection (8), of the Helmholtz equation.

Another alternative would be to use $v_x = \pm(1-\mathrm{i})\sqrt{\mu\omega\sigma_x/2}$ for all the x-derivatives, $v_y = \pm(1-\mathrm{i})\sqrt{\mu\omega\sigma_y/2}$ for all the y-derivatives, and $v_z = \pm(1-\mathrm{i})\sqrt{\mu\omega\sigma_z/2}$ for all the z-derivatives of the EM fields. However, our experience from exhaustive experiments on several different models indicates that the first choice gives better results. This could be due to a fact that the x-projection of the Helmholtz equation contains the x-directed conduction current $\sigma_x E_x$, hence σ_x may control the field derivatives better than the other two, σ_y and σ_z. Correspondingly, for the y- and z-projections of the Helmholtz equation.

Using these values of the exponents and the exponential FD approximation of all the second-order derivatives, the resulting discrete exponential FD formulation of eqs (6)–(8) on a staggered grid is given in Appendix C. The exponential FD approximation to the Helmholtz equation is used to form a matrix equation similar to eq. (12). The elements of the main diagonal of matrix **M** in both the standard and exponential FD methods are complex numbers. Off-diagonal elements of matrix **M** are real for the standard FD but complex for the exponential FD method.

TRUNCATION ERROR OF FD APPROXIMATIONS

In this section, we analyse the accuracy of both FD approximations by considering its local truncation error, assuming a coordinate dependence of the electric field that is typical for a homogenous conductive medium. In order to determine the expression for the truncation error for FD approximations, we follow the procedures introduced in Ixaru (1997) for the uniform grids in 1-D. We extend these procedures to the non-uniform grids for both non-mixed and mixed derivatives in 3-D. Using these procedures, the leading terms of the truncation error for the standard FD approximation of $\partial_y^2 E_x(\mathbf{r})$ and $\partial_y \partial_x E_y(\mathbf{r})$ are derived in Appendix D (eqs D1–D16, D23–D26 and D33). These leading terms read

$$\tau^{\mathrm{std}}_{2y}(\mathbf{r}) = -\frac{1}{3}\left(\Delta y_j - \Delta y_{j-1}\right)\partial_y^3 E_x(\mathbf{r}) - \frac{1}{12}\left(\Delta {y_j}^2 + \Delta {y_{j-1}}^2 - \Delta y_j \Delta y_{j-1}\right)\partial_y^4 E_x(\mathbf{r}), \tag{30}$$

and

$$\tau^{\mathrm{std}}_{2xy}(\mathbf{r}) = -\frac{1}{4}\left(\Delta y_j - \Delta y_{j-1}\right)\partial_x \partial_y^2 E_y(\mathbf{r}) - \frac{1}{24}\left(\Delta {y_j}^2 + \Delta {y_{j-1}}^2 - \Delta y_j \Delta y_{j-1}\right)\partial x \partial_y^3 E_y(\mathbf{r}) - \frac{1}{24}\Delta {x_i}^2 \partial_y \partial_x^3 E_y(\mathbf{r}), \tag{31}$$

respectively, for $\partial_y^2 E_x(\mathbf{r})$ and $\partial_y \partial_x E_y(\mathbf{r})$ at $(x_i + \frac{\Delta x_i}{2}, y_j, z_k)$. We have also verified that these leading terms for the standard FD approximations are exactly the same as the ones obtained using Taylor's series expansion of the fields, see for example Ferziger & Perić (2002) and Lynch (2005) for details to determine eqs (30) and (31) using Taylor's series. From eqs (30) and (31), one can see that the truncation error is of first-order for the non-uniform grid (i.e. $\Delta y_j \neq \Delta y_{j-1}$) and second-order for the uniform grid; this is a well-known result (Monk & Süli 1994; Ferziger & Perić 2002).

For the exponential FD approximations of $\partial_y^2 E_x(\mathbf{r})$ and $\partial_y \partial_x E_y(\mathbf{r})$ at $(x_i + \frac{\Delta x_i}{2}, y_j, z_k)$, the leading terms of the truncation errors are also derived in Appendix D (eqs D17–D22, D27–D28 and D34). These leading terms read

$$\tau_{2y}^{\exp}(\mathbf{r}) = A_1 \left(\partial_y^3 - \nu_y^2 \partial_y\right) E_x(\mathbf{r}) + A_2 \left(\partial_y^4 - \nu_y^2 \partial_y^2\right) E_x(\mathbf{r}), \tag{32}$$

$$\tau_{2xy}^{\exp}(\mathbf{r}) = C_1 \partial_x \left(\partial_y^2 - \nu_y^2\right) E_y(\mathbf{r}) + C_2 \partial_x \left(\partial_y^3 - \nu_y^2 \partial_y\right) E_y(\mathbf{r}) - \frac{1}{\nu_x^2}\left[\frac{\eta_0\left(\nu_x \frac{\Delta x_i}{2}\right) - 1}{\eta_0\left(\nu_x \frac{\Delta x_i}{2}\right)}\right] \partial_y \left(\partial_x^3 - \nu_x^2 \partial_x\right) E_y(\mathbf{r}) \tag{33}$$

with $\eta_0(\nu_x \frac{\Delta x_i}{2}) = \frac{1}{\nu_x \Delta x_i}[\exp(\nu_x \frac{\Delta x_i}{2}) - \exp(-\nu_x \frac{\Delta x_i}{2})]$, where the expressions for A_1, A_2, C_1 and C_2 are given in Appendix D, respectively, in eqs (D19), (D22), (D28) and (D28).

To analyse the leading terms of the exponential FD approximation, let us consider $\tau_{2y}^{\exp}(\mathbf{r})$ in the special case of a uniform grid with a constant cell size Δy (i.e. $\Delta y = \Delta y_j = \Delta y_{j-1}$). Then, eq. (32) becomes

$$\tau_{2y}^{\exp}(\mathbf{r}) = -\frac{1}{2\nu_y^2}\left[2 - \frac{\nu_y^2 \Delta y^2}{\eta_{-1}\left(\nu_y \Delta y\right) - 1}\right] \left(\partial_y^4 - \nu_y^2 \partial_y^2\right) E_x(\mathbf{r}), \tag{34}$$

where $\eta_{-1}(\nu_y \Delta y) = \frac{1}{2}[\exp(\nu_y \Delta y) + \exp(-\nu_y \Delta y)]$.

The corresponding leading term of the truncation error for the standard FD approximation (eq. 30) for the uniform grid becomes

$$\tau_{2y}^{\mathrm{std}}(\mathbf{r}) = -\frac{1}{12} \Delta y^2 \partial_y^4 E_x(\mathbf{r}). \tag{35}$$

We now compare these two expressions of the truncation errors for the two FD methods for an electric field $E_x(\mathbf{r})$ having dependence typical for CSEM. Let us consider an x-oriented horizontal electric dipole (HED) (a small current element of length $\mathrm{d}l$) with the electric current I, placed at the origin in a uniform homogeneous medium. An exact expression for the broadside electric field due to this HED can be obtained following Ward & Hohmann (1988, p. 173) as

$$E_x(y) = \frac{I\,\mathrm{d}l}{4\pi\sigma y^3}\left(k^2 y^2 - \mathrm{i}ky - 1\right) \exp(-\mathrm{i}ky). \tag{36}$$

Here, $E_x(y)$ represents the electric field which is directed along x, and taken at different positions y, while $x = z = 0$. Using this simple expression, we can analytically compute derivatives of any order, for example $\partial_y E_x(y)$, $\partial_y^2 E_x(y)$, $\partial_y^3 E_x(y), \ldots$, and hence also the leading terms of the truncation error in eqs (34) and (35) for both FD approximations of $\partial_y^2 E_x(y)$.

Fig. 2 shows the truncation errors, $\tau_{2y}^{\mathrm{std}}(\mathbf{r})$ and $\tau_{2y}^{\exp}(\mathbf{r})$, normalized to the derivative $\partial_y^2 E_x(y)$ and plotted against cell sizes Δy at four different offsets, $y = 4\delta$, 8δ, 12δ and 16δ; the cell sizes and offsets are normalized to the skin depth $\delta = \sqrt{2/\mu\omega\sigma}$. From these plots, we notice that truncation error curve for the exponential FD is almost parallel to the standard FD curve. The truncation error in the standard FD approximation is of second-order (see eq. 35). Hence, the truncation error in the exponential FD approximation is also approximately second-order. Indeed, this second-order accuracy can exactly be demonstrated in the limit of small Δy, when eq. (34) becomes

$$\tau_{2y}^{\exp}(\mathbf{r}) = -\frac{1}{12} \Delta y^2 \left(\partial_y^4 - \nu_y^2 \partial_y^2\right) E_x(\mathbf{r}), \tag{37}$$

since $\eta_{-1}(\nu_y \Delta y) \approx 1 + \frac{1}{2!}\nu_y^2 \Delta y^2 + \frac{1}{4!}\nu_y^4 \Delta y^4$. Interestingly, the plots show that even at larger Δy the truncation error in the exponential FD method also behaves very close to the second-order.

Fig. 2 shows that though both methods are essentially second-order, the truncation error in the exponential FD method can be much smaller, especially at longer offsets. The respective truncation error in the exponential FD method at offsets $y = 4\delta$, 8δ, 12δ and 16δ (corresponding to the four plots of Fig. 2) is approximately 2, 5, 8 and 10 times smaller than for the standard FD method. It follows from eqs (35) and (37) that in the limit of small Δy, the truncation errors in both FD methods have the same cell size dependence and differ only in the offset dependent part: the standard FD has $\partial_y^4 E_x(\mathbf{r})$, while exponential FD has $(\partial_y^4 - \nu_y^2 \partial_y^2) E_x(\mathbf{r})$. Thus, the accuracy improvement of the exponential FD truncation error is mainly due to the offset dependent part. This improvement is obvious if $E_x(y)$ is a plane wave proportional to $\exp(-\mathrm{i}ky)$, since then $(\partial_y^4 - \nu_y^2 \partial_y^2) E_x(\mathbf{r})$ identically vanishes for $\nu_y = -\mathrm{i}k$. For a dipole source, the fields, for example that given by eq. (36), are proportional to exponential terms as well as rational expressions. At shorter offsets, the rational expressions dominate, while at longer offsets, the exponential terms dominate. Therefore, it is expected that the fields due to a dipole source are well approximated using the exponential FD method at longer offsets, and hence have small truncation errors, which is in agreement with the plots.

To follow the behaviour of truncation errors from very near to very far offsets, we have also plotted the truncation errors in both FD approximations against the offsets at a given cell size $\Delta y = 0.1\delta$; this is shown in Fig. 3. For both methods, the truncation error increases towards shorter offsets because closer to the source the fields vary faster and the FD approximations become less accurate. At very near offsets $y < 2\delta$, the truncation errors for both FD methods are very similar. However, at offsets $y > 2\delta$, the exponential FD method shows a very clear improvement; the truncation error in the exponential FD method decreases significantly with the offset, while in standard FD method the truncation error remains almost constant. This is also in agreement with the above discussion because at longer offsets, the electric field in eq. (36) is dominated by the exponential term $\exp(-\mathrm{i}ky)$, which is well approximated by the exponential FD method. These results clearly motivate us to perform 3-D EM modelling using the exponential FD method.

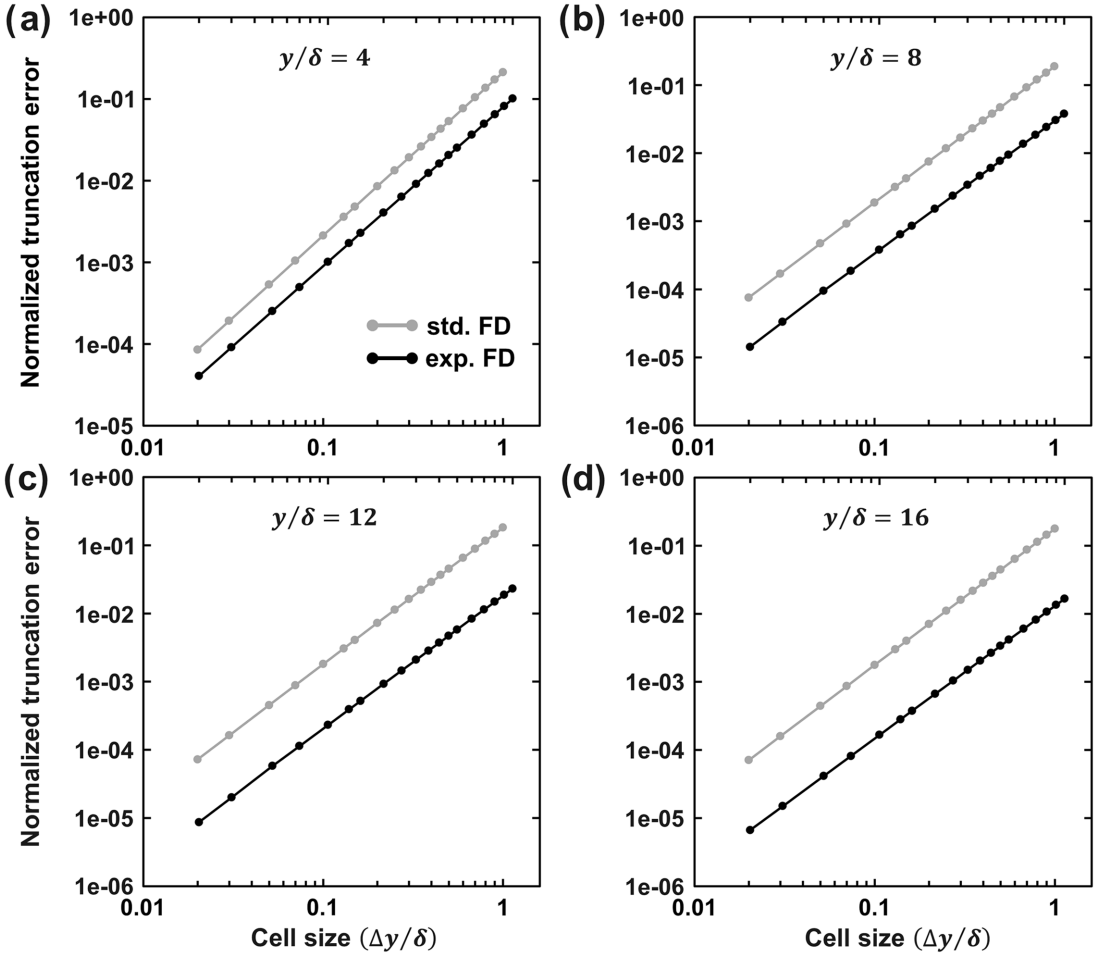

Figure 2. Truncation errors for the standard FD τ_{2y}^{std} (grey curve) (eq. 35) and the exponential FD τ_{2y}^{exp} (black curve) (eq. 34), normalized to the derivative $\partial_y^2 E_x(y)$ and plotted as a function of different cell sizes $(\Delta y/\delta)$ at different offsets: (a)$y/\delta = 4$, (b) $y/\delta = 8$, (c) $y/\delta = 12$ and (d) $y/\delta = 16$. The offsets and cell sizes are normalized with respect to the skin depth δ. The expression of $E_x(y)$ is given in eq. (36). The truncation errors in both methods are of second-order, but they are always smaller in exponential FD.

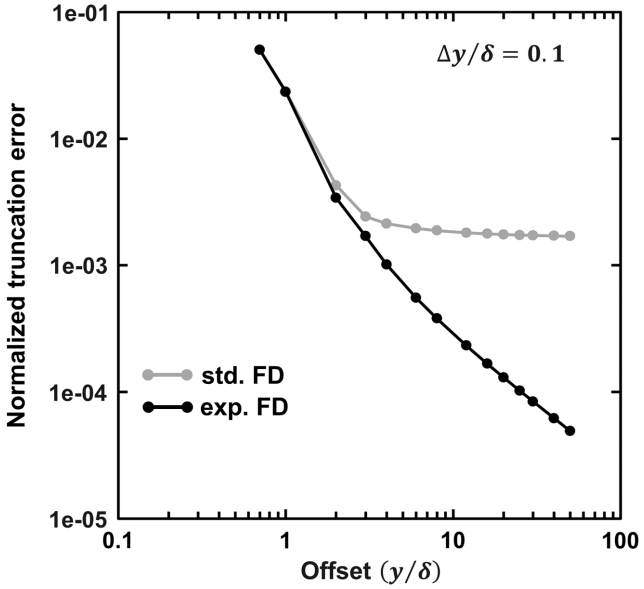

Figure 3. Truncation errors for the standard FD τ_{2y}^{std} (grey curve) (eq. 35) and the exponential FD τ_{2y}^{exp} (black curve) (eq. 34), normalized to the derivative $\partial_y^2 E_x(y)$ and plotted as a function of offsets (y/δ) at a given cell size $\Delta y/\delta = 0.1$. The expression of $E_x(y)$ is given in eq. (36). It can be observed that the advantage of exponential FD method is most pronounced at longer offsets.

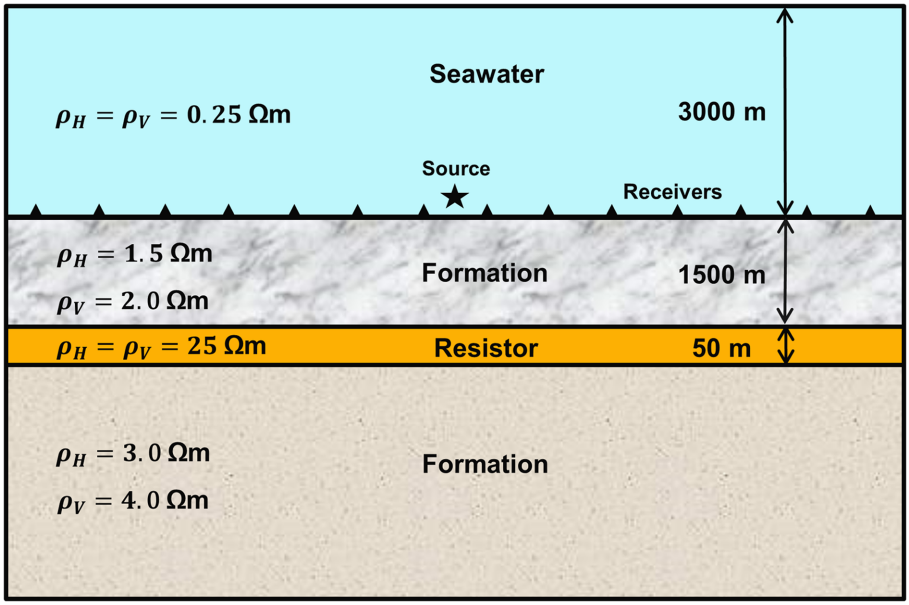

Figure 4. Vertical cross-section of a deep-water layered earth model used for CSEM modelling with receivers at the sea bed and a HED source 30 m above it. $\rho_H = 1/\sigma_x = 1/\sigma_y$ and $\rho_V = 1/\sigma_z$ represent, respectively, the horizontal and vertical resistivities.

RESULTS

In this section, we compare the efficiency of the standard and exponential FD methods in three marine CSEM scenarios: (1) deep-water, (2) shallow-water and (3) intermediate water depth. The shallow-water and intermediate water depth cases need a special consideration because of the presence of the air layer that has an extremely high resistivity and plays a very important role for EM signal propagation.

Deep-water layered earth model

Let us consider the layered earth model depicted in Fig. 4 to compare the efficiency of the exponential and standard FD methods. The model is vertical transverse isotropic (VTI), that is the conductivity tensor is diagonal and the horizontal conductivity values σ_x and σ_y are equal. The source is an x-oriented HED with a frequency of 1 Hz and placed 30 m above the seabed. The dimension of the model in Fig. 4 is $20 \times 20 \times 8$ km^3. We shall refer to this domain as the 'domain of interest' which includes the source and receivers. The domain of interest was discretized using non-uniform grids. Away from the source the cell size increased according to a power law $\mathrm{d}h(n) = \min(\mathrm{d}h_{\min} \times \lambda^{n-1},\ \mathrm{d}h_{\max})$ where $h = x$, y, or z; $n = 1, 2, \ldots\ldots$ is a cell counter; $\mathrm{d}h_{\min}$ is the minimum cell size; $\mathrm{d}h_{\max}$ is the maximum cell size; and λ is a constant growth factor. Values of λ were determined by $\mathrm{d}h_{\min}$, $\mathrm{d}h_{\max}$, number of cells and distance from the source to the model boundaries. The cell sizes were chosen finer near the source in order to better accommodate for the rapid variation of the EM fields in that region.

The computational domain was extended by adding 15 km padding at the vertical and bottom boundaries of the domain of interest to reduce the errors due to truncation of the unbounded domain. The horizontal and vertical resistivities of this padding are the same as the corresponding resistivities at the model boundaries. We refer to this additional padding as the 'extended domain'. One would normally add an air layer at the top boundary but this was not done in our deep-water cases since for 1 Hz frequency used in the analysis below, the skin depth in seawater (with $\sigma = 4$ S m^{-1}) is just ~ 250 m. Hence, the amplitudes of the EM fields, having diffused about twelve skin depth in the seawater, are reduced by 99.9994 per cent at the sea surface and ignoring the air layer has negligible effect on the computed CSEM response. The extended domain was discretized with severely stretched non-uniform cells following a similar power law as above, but with a larger λ. Table 1 specifies the seven different grids used to discretize the domain of interest and extended domain by listing the corresponding λ values, minimum and maximum cell sizes in the domain of interest, number of cells and resulting number of unknowns. In the extended domain, the minimum cell sizes are equal to the corresponding maximum cell sizes in the domain of interest and the maximum cell size is 1600 m.

All simulations were carried out sequentially on a computer with Intel Xeon CPU E5-2690 processors running at 2.90 GHz and 264 GB of memory. The resulting matrix equations were solved using the above mentioned iterative solver. The iterations were stopped when the residual norms ($\|\mathbf{Mx} - \mathbf{s}\|$) dropped by a factor 10^{-9} from its original value for a zero-solution (i.e. $\|\mathbf{s}\|$). Table 2 shows the run time statistics for the modelling jobs using the standard and exponential FD methods. It can be observed that the solver took similar time to solve the linear systems for both FD methods, however, the exponential FD method took somewhat longer time to assemble the matrices than the standard FD method. The reason for the relatively longer matrix assembly time for the exponential FD method is the fact that the computation of non-zero coefficients in the matrix involves complex exponential functions. This is however not critical since the matrix assembly time was always much shorter than the corresponding solution time.

Table 1. Details of the grids used to discretize the layered earth models for FD CSEM simulations. Here in x-, y- and z directions, respectively, λ_x, λ_y and λ_z are the constant growth factors, $dx_{\min}$, $dy_{\min}$ and $dz_{\min}$ are the minimum cell sizes, $dx_{\max}$, $dy_{\max}$ and $dz_{\max}$ are the maximum cell sizes, and N_x, N_y and N_z are the number of cells, while $3N = 3N_xN_yN_z$ is the total number of unknowns. The domain of interest refers to the main computational volume, which includes the source and receivers; whilst the extended domain refers to the padding added at the model boundaries to reduce the errors due to truncation of the unbounded domain. In the extended domain, the minimum cell sizes are equal to the corresponding maximum cell sizes in the domain of interest, while the maximum cell size is 1600 m in all directions, and $\lambda_x = \lambda_y = \lambda_z = \lambda$.

	Domain of interest								Extended domain			
Grids	$\lambda_x = \lambda_y$	$dx_{\min} = dy_{\min}$ (m)	$dx_{\max} = dy_{\max}$ (m)	λ_z	$dz_{\min}$ (m)	$dz_{\max}$ (m)	$N_x = N_y$	N_z	λ	$N_x = N_y$	N_z	$3N$
G-1	1.005	40	90	1.017	20	72	332	164	1.12	52	28	84 934 656
G-2	1.008	60	150	1.026	20	125	212	136	1.12	44	24	31 457 280
G-3	1.019	60	270	1.039	20	200	156	108	1.12	36	20	14 155 776
G-4	1.039	70	440	1.051	30	250	98	78	1.12	30	18	4 718 592
G-5	1.065	80	680	1.058	42	360	70	65	1.12	26	15	2 211 840
G-6	1.073	100	780	1.079	42	450	60	52	1.2	20	12	1 228 800
G-7	1.096	120	1000	1.085	80	500	48	38	1.2	16	10	589 824

Table 2. Runtime statistics for CSEM modelling with the standard and exponential FD methods for the deep-water layered earth model on the different grids defined in Table 1. The number of iterations is that required for the relative residual norm to drop below 10^{-9} in the iterative solver. Here 'Std.' and 'Exp.' are abbreviations for 'standard' and 'exponential', respectively.

		Matrix assembly time (s)		Number of iterations		Linear system solution time (s)	
Grids	Number of unknowns	Std. FD	Exp. FD	Std. FD	Exp. FD	Std. FD	Exp. FD
G-1	84 934 656	192.7	363.6	3	3	1535.6	1539.1
G-2	31 457 280	47.8	106.7	4	4	737.0	734.9
G-3	14 155 776	7.6	46.3	5	5	422.3	419.9
G-4	4 718 592	1.7	15.1	7	7	176.9	181.0
G-5	2 211 840	0.9	4.0	9	9	107.0	110.2
G-6	1 228 800	0.5	3.9	6	7	41.0	45.1
G-7	589 824	0.2	1.8	6	7	19.8	22.4

We compare the 3-D simulation results obtained through the standard and exponential FD methods to reference fields calculated using a semi-analytical plane-layer method (Løseth & Ursin 2007). Figs 5(a) and (b), respectively, show the amplitude and phase responses for the x- and z-components of the electric field and the y-component of the magnetic field computed along an inline receiver line located at the seabed. The grey curve, black curve and circles, respectively, show results obtained with the standard FD, exponential FD and plane-layer methods. All the three datasets are almost indistinguishable on this scale, therefore it is more instructive to look at the normalized amplitude and phase difference plots. The normalized amplitudes and phase differences between results obtained with the plane-layer method, and results obtained via the standard and exponential FD methods on the finest grid (labelled G-1 in Table 1) are plotted, respectively, in Figs 5(c) and (d) for the inline fields. Except for the responses that are close to the source position, the field amplitudes differ at most by 0.3 per cent and the phases at most by 0.8° in both methods. Hence both methods provide good accuracy for a very fine grid.

We now examine how much the accuracy degrades for each method for fields computed on coarse grids G-2 to G-7 defined in Table 1. The normalized amplitudes and phase differences between results obtained with the plane-layer method, and results obtained via the standard and exponential FD methods on grid G-3 are shown, respectively, in Figs 6(a) and (b). It is evident that the exponential FD method gives more accurate results than the standard FD method. A similar behaviour is observed in Figs 6(c) and (d) showing data for grid G-4.

It is also useful to compute the average relative errors based on the following expression:

$$\epsilon = \frac{1}{p}\sum_{i=1}^{p}\sqrt{\frac{|F_1(\mathbf{r}_i) - F_2(\mathbf{r}_i)|^2}{\left(|F_1(\mathbf{r}_i)|^2 + |F_2(\mathbf{r}_i)|^2\right)/2 + \alpha^2}}, \tag{38}$$

where F is either E_x, E_z or H_y, subscript 1 represents fields computed with the plane-layer method, and subscript 2 represents fields computed with the standard or exponential FD method; p is number of receivers; $\mathbf{r}_i$ is the position of the ith receiver; and α is the ambient noise level. The sources of ambient noise could be MT signals, swell noise, or receiver self-noise (Constable & Weiss 2006). Table 3 shows typical values of α chosen following Mittet & Morten (2013) for different seawater depths. The noise level increases with the reduction in the seawater depth.

Fig. 6(e) shows the relative errors, averaged over all of the inline offsets from −10 to 10 km, for E_x, E_z and H_y for all the grids from G-1 to G-7 where they are plotted as a function of the number of unknowns. Different number of unknowns correspond to seven different grids defined in Table 1. From these plots, we observe that the average relative errors in both FD methods are almost identical when the number of unknowns is very large (grid G-1). However, for E_x and H_y on coarse grids G-2 to G-7, the average relative errors for the exponential FD method are nearly two to three times smaller than for the standard FD method on the same grids. For E_z, the improvement achieved by the exponential FD method is slightly less significant than for E_x and H_y, but E_z is in fact much more seldom used in the marine CSEM

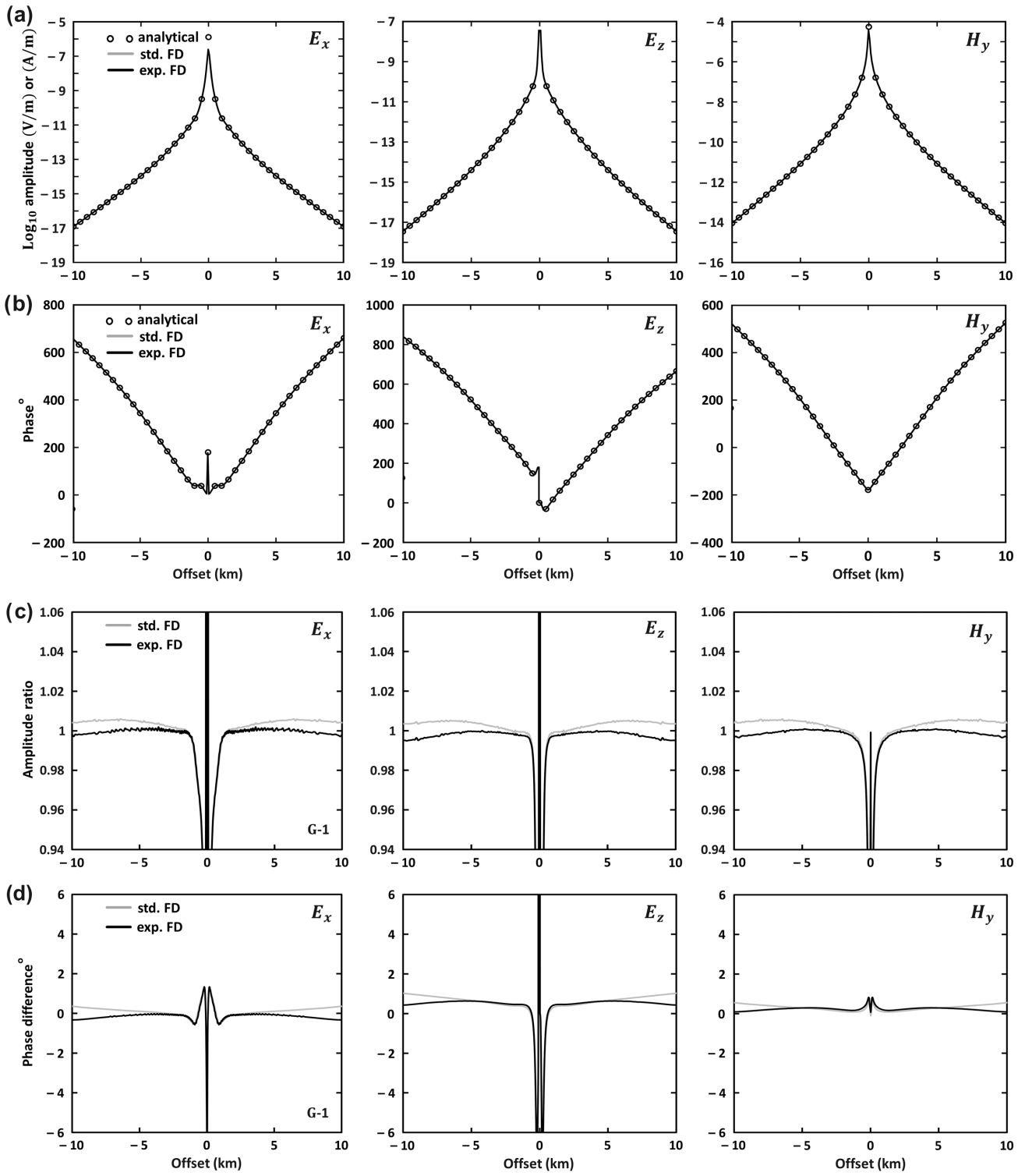

Figure 5. (a) Amplitude and (b) phase responses of E_x, E_z and H_y at 1 Hz as a function of source-receiver offset for the deep-water layered earth model of Fig. 4. They are calculated using the standard (grey curve) and exponential (black curve) FD methods, as well as the semi-analytical plane-layer modelling of Løseth & Ursin (2007) (circles). (c) Normalized amplitudes and (d) phase differences with respect to semi-analytical plane-layer modelling for the fields in (a) and (b). The FD results are computed on grid G-1 defined in Table 1.

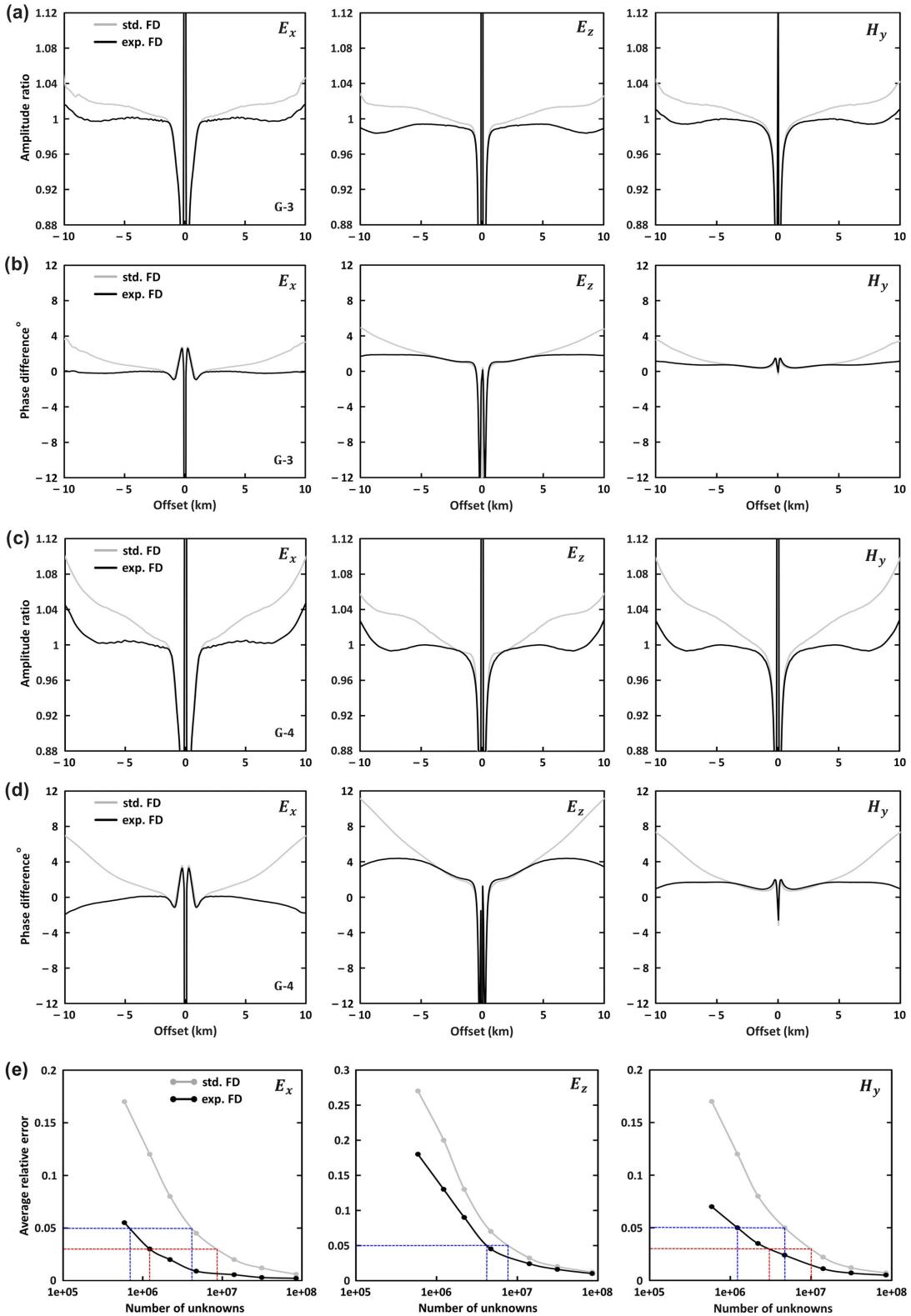

Figure 6. (a) Normalized amplitude and (b) phase difference for E_x, E_z and H_y similar to those in Figs 5(c) and (d), but computed using coarse grid G-3. Panels (c) and (d) show similar plots for the even coarser grid G-4. Results obtained with the exponential FD method are more accurate for most offsets. This is also illustrated in panel (e) showing the relative error averaged over all offsets, eq. (38), as a function of the number of unknowns for all grids defined in Table 1.

Table 3. Typical values of the ambient noise level chosen following Mittet & Morten (2013): α_E and α_H are the noise levels in the electric and magnetic fields, respectively.

	Ambient noise level (α)	
Seawater depth (m)	α_E (V m^{-1})	α_H (A m^{-1})
3000	7×10^{-17}	7×10^{-14}
500	4×10^{-16}	4×10^{-13}
200	8×10^{-16}	8×10^{-13}

method. For example, for grid G-3, the average relative errors for E_x, E_z and H_y for the exponential FD method are 0.6, 2.4 and 1.1 per cent, respectively, while for the standard FD method they are larger: 1.9, 3.1 and 2.1 per cent. For grid G-4, the average relative errors for E_x, E_z and H_y are, respectively, 1, 4.7 and 2.4 per cent for the exponential FD method and 4.2, 6.8 and 4.9 per cent for the standard FD method.

The above results show that the exponential FD method gives more accurate results than the standard FD method on the same grid. This implies that the exponential FD method can achieve the same accuracy with a coarser grid and hence is faster than the standard FD method. To demonstrate this, let us consider a maximum allowed average relative error of 5 per cent. To compute E_x with this error, the standard FD requires about 4.2 million unknowns while exponential FD requires only 0.7 million unknowns (see blue lines in Fig. 6e). The corresponding modelling times would be about 164 and 26 s, respectively, for the standard and exponential FD methods. For H_y with the same error, the standard and exponential FD methods require, respectively, 4.7 million and 1.2 million unknowns, respectively corresponding to modelling times of 179 and 49 s. Similarly for E_z, the standard and exponential FD methods require, respectively, 8 and 4 million unknowns, respectively corresponding to modelling times of 268 and 170 s.

If the maximum allowed average relative error is 3 per cent then to compute E_x, the standard and exponential FD methods require, respectively, 8.2 and 1.2 million unknowns (see red lines in Fig. 6e), respectively corresponding to modelling times of 275 and 49 s. Similarly for H_y, the standard and exponential FD methods require, respectively, 10 and 3 million unknowns, respectively corresponding to modelling times of 340 and 132 s. Here, the modelling times were interpolated using Table 2 in combination with Fig. 6(e). It is clear that the exponential FD method requires approximately two to six times less unknowns or 1.5 to six times shorter modelling times as compared to the standard FD method for the same accuracy. It should be noted that the savings in modelling time would be even larger if one used a sparse direct solver since the number of floating point operations required for factorization scales with the number of unknowns as $\mathcal{O}(N^2)$, while for an iterative solver the scaling is approximately linear.

3-D deep-water geological model: Gulf of Mexico

In the previous example, the results were obtained for a simplistic earth model with 1-D resistivity distribution, which is favourable for the exponential FD method that should be especially efficient for large uniform regions. Inside these regions, the spatial dependence of EM fields is dominated by the exponential factor e^{ikr}, at least at long offsets, and thus should be well approximated by the exponential basis functions. However, in real world the models have a 3-D structure and a high degree of inhomogeneity. Therefore, it is important to know whether the proposed exponential FD method can achieve significant improvements also for realistic 3-D cases.

Fig. 7 shows the horizontal and vertical resistivities for a realistic deep-water 3-D model taken from the Perdido fold belt in the northwestern Gulf of Mexico, with northeast-southwest trending anticlines. The seawater depth is about 3 km with resistivities in the range

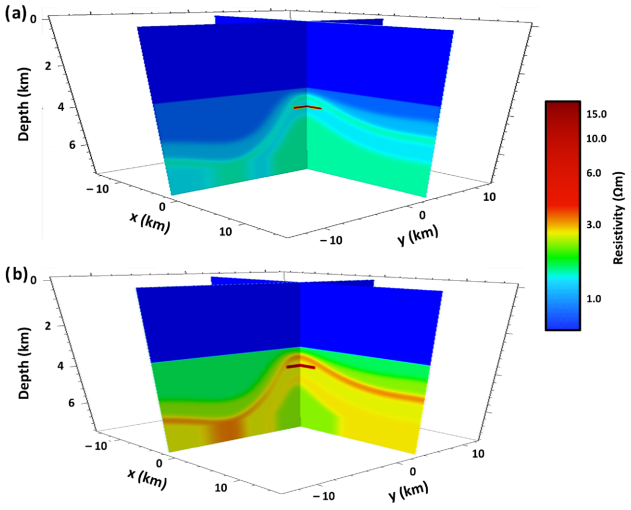

Figure 7. (a) Horizontal and (b) vertical resistivity cross-sections from a deep-water Gulf of Mexico model.

Table 4. Details of the grid used to discretize the 3-D deep-water geological model for FD CSEM simulations. We use the same nomenclature as in Table 1 and the same parameters for the extended domain except that the maximum cell size here is 800 m.

Domain of interest												Extended domain			
λ_x	dx_{min} (m)	dx_{max} (m)	λ_y	dy_{min} (m)	dy_{max} (m)	λ_z	dz_{min} (m)	dz_{max} (m)	N_x	N_y	N_z	λ	N_x	N_y	N_z
1.004	20	90	1.012	50	200	1.017	20	82	702	242	159	1.06	66	46	33

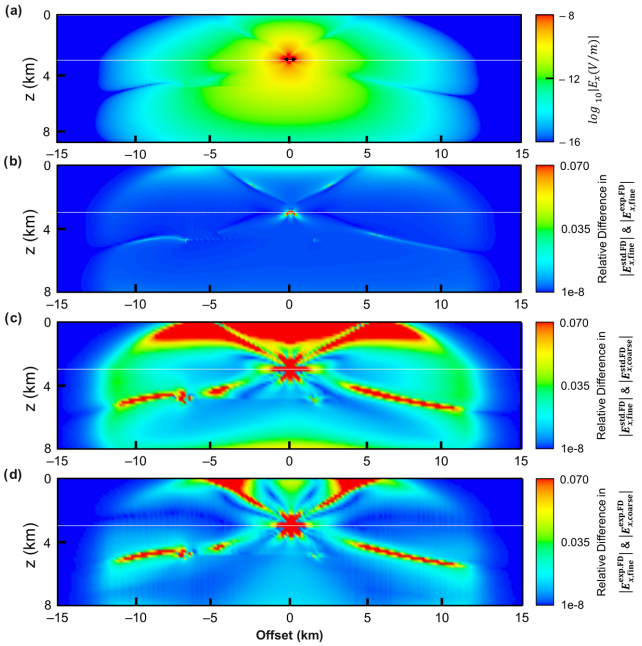

Figure 8. Inline vertical slices showing the CSEM modelling results for the E_x field component, for the deep-water model from the Gulf of Mexico in Fig. 7. (a) Amplitude response on a log scale; (b) relative difference in amplitudes computed using standard and exponential FD methods, both on a very fine grid with 768 × 288 × 192 cells. (c) Relative difference in amplitudes computed on the fine (768 × 288 × 192 cells) and coarse (256 × 288 × 64 cells) grids using the standard FD method. (d) The same as (c), but for the exponential FD method. Comparison of (c) and (d) shows that the proposed exponential method is more accurate.

0.2–0.3 Ωm; whereas the formation horizontal and vertical resistivities, respectively vary in the ranges 1.0–2.0 Ωm and 1.5–3.0 Ωm. The model includes a resistive oil reservoir whose horizontal and vertical resistivities are 15.0 and 18.0 Ωm, respectively. The dimension of the model is $30 \times 26 \times 8$ km^3. The computational domain was extended by adding 10 km padding at the vertical and bottom boundaries of the domain of interest. The domain of interest and extended domain were discretized using the previously described power law for the non-uniform grid sizes. Table 4 shows the details of the grid used to discretize the domain of interest and extended domain. The discretization of the FD grid model results in 768 × 288 × 192 cells, representing approximately 127 million degrees of freedom. The source is an x-oriented HED with a frequency of 1 Hz and located 30 m above the flat seabed.

The accuracy of our standard FD modelling code for similar 3-D models has been validated in our previous paper Jaysaval *et al*. (2014) by comparing our simulation results against results obtain using a fast FD time-domain modelling code.

The matrix assembly and linear system solution times were 302 and 3692 s for the standard FD method, and 425 and 3656 s for the exponential FD method. For both methods, the iterative solver needed five iterations to allow the relative residual norm to become smaller than 10^{-9}. Figs 8(a) and 9(a) show the amplitude responses, respectively, for E_x and E_z. The white lines indicate the seafloor at about 3 km depth and the black arrows indicate the source position. These figures show that the amplitudes of EM fields resulting from a 1 Hz HED source rapidly decrease with increasing distance from the source. Fig. 8(b) shows the relative difference in E_x amplitude computed by the standard and exponential FD methods, while Fig. 9(b) shows the same for E_z. The relative amplitude difference, averaged over the whole model, is less than 0.5 per cent. Hence we again observe that the standard and exponential FD methods give almost identical results on a very fine grid. Note that this remains true even though the cell sizes in the y-direction were somewhat coarser than in the x- and z-directions. We tested the effect of different cell sizes in the y-direction and found only minor effect in the accuracy, provided that the cell sizes were not chosen excessively coarse. For example, the average relative amplitude difference between modelled results with the standard and exponential FD methods when going from ($\lambda_y = 1.009$, $dy_{min} = 30$ m, $dy_{max} = 150$ m) to ($\lambda_y = 1.022$, $dy_{min} = 60$ m, $dy_{max} = 300$ m) was between 0.4 and 0.7 per cent. Hence the grid specified in Table 4 is fine enough in the y-direction to provide good accuracy.

We shall now illustrate the efficiency improvements of the exponential FD method against the standard FD method for coarser grids. Due to unavailability of analytical solutions for 3-D models, we assume the results obtained using the above fine grid with 768 × 288 × 192 cells are a good approximation to the exact solution. These fine grid results are then compared against coarse grid results obtained using

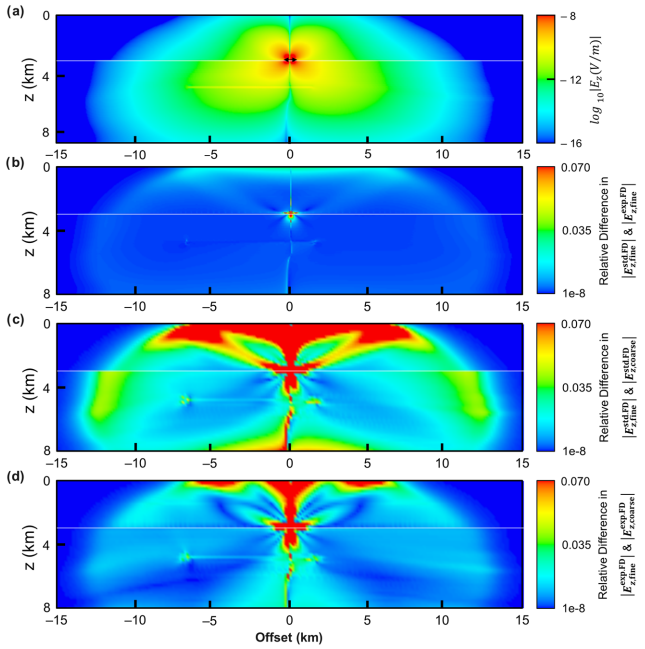

Figure 9. The same as Fig. 8, but for the E_z field component. Comparison of (c) and (d) shows that the proposed exponential method is more accurate also for E_z.

both FD methods. The coarse grid model is obtained from the fine grid model by merging each successive three cells together in the x- and z-directions but no merging is done in the y-direction where the cell sizes were already chosen quite coarse. The resulting coarse grid discretized model has $256 \times 288 \times 64$ cells, representing approximately 14.2 million degrees of freedom. The matrix assembly and linear system solution times were 11 and 434 s for the standard FD method and 52 and 428 s for the exponential FD method. For both methods, the iterative solver again needed five iterations to allow the relative residual norm to drop below 10^{-9}.

The relative amplitude differences between the fine and coarse grid results obtained using the standard FD are shown in Figs 8(c) and 9(c), respectively, for E_x and E_z. Figs 8(d) and 9(d) show the same relative errors, respectively, for E_x and E_z but computed using the exponential FD method. Comparison of these relative amplitude difference images reveals that the exponential FD method provides more accurate results as compared to the standard FD method on the same grid. For example, the relative amplitude differences in the seawater and near the seafloor (at intermediate-to-long offsets) were significantly reduced in the exponential FD method. In addition, the exponential FD results were improved in the formation at long offsets and central deeper part of the model as compared to the standard FD results. The average values of the relative amplitude difference between the fine and coarse grid results for E_x and E_z are, respectively, 3.2 and 3.8 per cent for the standard FD method and 1.7 and 2.1 per cent for the exponential FD method.

Shallow-water layered earth model

To examine the performance of the exponential FD method for shallow-water cases, we built a shallow-water resistivity model from the deep-water layered earth model by simply removing 2.8 km of seawater so that the water layer becomes only 200 m thick. The source is again an x-oriented HED with a frequency of 1 Hz placed 30 m above the seabed. For shallow-water models, it is essential to include a thick air layer above the sea surface; therefore, the top boundary of the computational domain included an air layer of thickness ~50 km and resistivity 10^6 Ωm. In addition, 30 km padding was added at the vertical and bottom boundaries of the domain of interest. Note that, for shallow-water models, the computational domain boundaries are required to be placed even farther from the source as compared to those for deep-water models. This is in order to make sure the combination of a strong shallow-water airwave and zero-field Dirichlet boundary conditions does not lead to edge effects. The airwave is the signal component that diffuses upward through the seawater from the source to the sea surface, then propagates as a 'wave' horizontally through the air before diffusing back down through the seawater to the receiver (Nordskag & Amundsen 2007).

The air layer was discretized with 20 horizontal layers of cells; the cell thickness increased rapidly according to the power law defined above with $\lambda = 1.28$ and the minimum cell thickness of 80 m at the air-water interface. The domain of interest was again discretized using the same grids from G-1 to G-7 described in Table 1 except for discretization in the z-direction. For this model in the z-direction, we have only 200 m of seawater, formation, resistor and the additional air layer; the seawater was discretized using the same λ_z value as in Table 1 but with minimum cell sizes of 20 and 50 m, respectively, for grids G-1 to G-4 and G-5 to G-7, while the formation and resistor were discretized using the same parameters as in Table 1. The number of cells and unknowns remains the same as given in Table 1. Here, the extended domain

Table 5. Runtime statistics for CSEM modelling with the standard and exponential FD methods for the shallow-water (200 m) layered earth model on the different grids defined in Table 1. The iterations were stopped when the relative residual norms dropped below 10^{-8}. Here 'Std.' and 'Exp.' are abbreviations for 'standard' and 'exponential', respectively.

		Matrix assembly time (s)		Number of iterations		Linear system solution time (s)	
Grids	Number of unknowns	Std. FD	Exp. FD	Std. FD	Exp. FD	Std. FD	Exp. FD
G-1	84 934 656	225.3	333.2	69	71	32387.9	32925.6
G-2	31 457 280	49.8	101.7	56	57	10698.3	10728.6
G-3	14 155 776	5.7	45.9	36	41	3185.2	3625.3
G-4	4 718 592	1.8	15.1	19	20	566.5	602.3
G-5	2 211 840	0.9	7.1	11	12	158.0	185.2
G-6	1 228 800	0.6	3.9	15	16	111.6	119.5
G-7	589 824	0.2	1.7	16	17	51.6	53.2

was also discretized with severely stretched non-uniform cells as previously but with the maximum cell size of 4000 m and $\lambda = 1.16$ and 1.24, respectively, for grids G-1 to G-4 and G-5 to G-7.

Table 5 shows the run time statistics for the shallow-water modelling jobs using the standard and exponential FD methods. The matrix assembly times for both methods were very similar to the corresponding matrix assembly times in the deep-water layered earth model. However, the convergence rate of the solver became significantly slower than for the deep-water model, see Table 2, particularly for the finer grids. The reason for the slow convergence is ill-conditioning of the matrices resulting from large aspect ratios of the cells in the air layer and thick boundary paddings. The very high resistivities in the air layer are an additional reason—this gives a large null-space to the curl–curl operator (Mulder 2006). Due to slow convergence of the solver for shallow-water models, the iterations were chosen to stop when the relative residual norms drop below 10^{-8} instead of 10^{-9} as for deep-water models. This choice of the convergence criteria also provides very good accuracy of computed fields as can be seen in the following results.

Figs 10(a) and (b) show the amplitude and phase responses of E_x, E_z and H_y computed on a coarse grid G-3 along an inline receiver line located at the seabed. The normalized amplitudes and phase differences between results obtained with the plane-layer method, and results obtained via the standard and exponential FD methods on grid G-3 are plotted, respectively, in Figs 10(c) and (d). These figures show that the numerical errors in both FD methods are very similar. We now compute the relative errors, averaged over all of the inline offsets from -10 to 10 km, using eq. (38) and α values from Table 3. These average relative errors have very similar values for both methods: 1.6, 2.8 and 1.3 per cent, respectively, for E_x, E_z and H_y.

The results obtained on coarse grid G-3, unlike the deep-water results, show no improvements by using the exponential FD method against the standard FD method. Therefore, we calculate average relative errors for the fields computed using both FD methods on all other grids from G-1 to G-7 to see if there exists any improvements on them. Fig. 10(e) shows plots of relative errors, averaged over all of the inline offsets from -10 to 10 km, for E_x, E_z and H_y as a function of the number of unknowns for the standard and exponential FD methods. Also from these plots, one can hardly notice any improvements due to the use of the exponential FD method and both methods have very similar average relative errors.

Intermediate water depth layered earth model

In the previous examples, we examined the performance of the exponential FD method against the standard FD method for the deep-water and shallow-water cases. We now examine the same for an intermediate water depth case. We built an intermediate water depth model from the deep-water layered earth model by removing 2.5 km of seawater so that the water layer becomes only 500 m thick. The source parameters, air layer, boundary extensions and discretization were similar to the previous shallow-water model example. The differences were only in the seawater thickness, now 500 m, and its discretization parameters which were the same as in Table 1. Table 6 gives run time statistics for the modelling jobs using the standard and exponential FD methods. The matrix assembly times for both methods were also very similar to the corresponding matrix assembly times in the previous layered earth model examples. The convergence rate of the solver improved as compared to the shallow-water model with 200 m of seawater.

Figs 11(a) and (b) show the amplitude and phase responses, respectively, and Figs 11(c) and (d), respectively, show the normalized amplitudes and phase differences between the responses computed with the plane-layer method, and standard and exponential FD methods on grid G-3. Figs 11(c) and (d) show that no major improvements in the numerical results on grid G-3 by using the exponential FD method as compared to the standard FD method. Fig. 11(e) shows plots of relative errors, averaged over all of the inline offsets from -10 to 10 km, for the inline fields as a function of the number of unknowns for standard and exponential FD methods; the selected values of α are shown in Table 3 for 500 m of seawater. From these plots, we observe that the exponential and standard FD methods provide similar accuracy for the finer grids, but the exponential FD method gives slightly better results on the coarser grids.

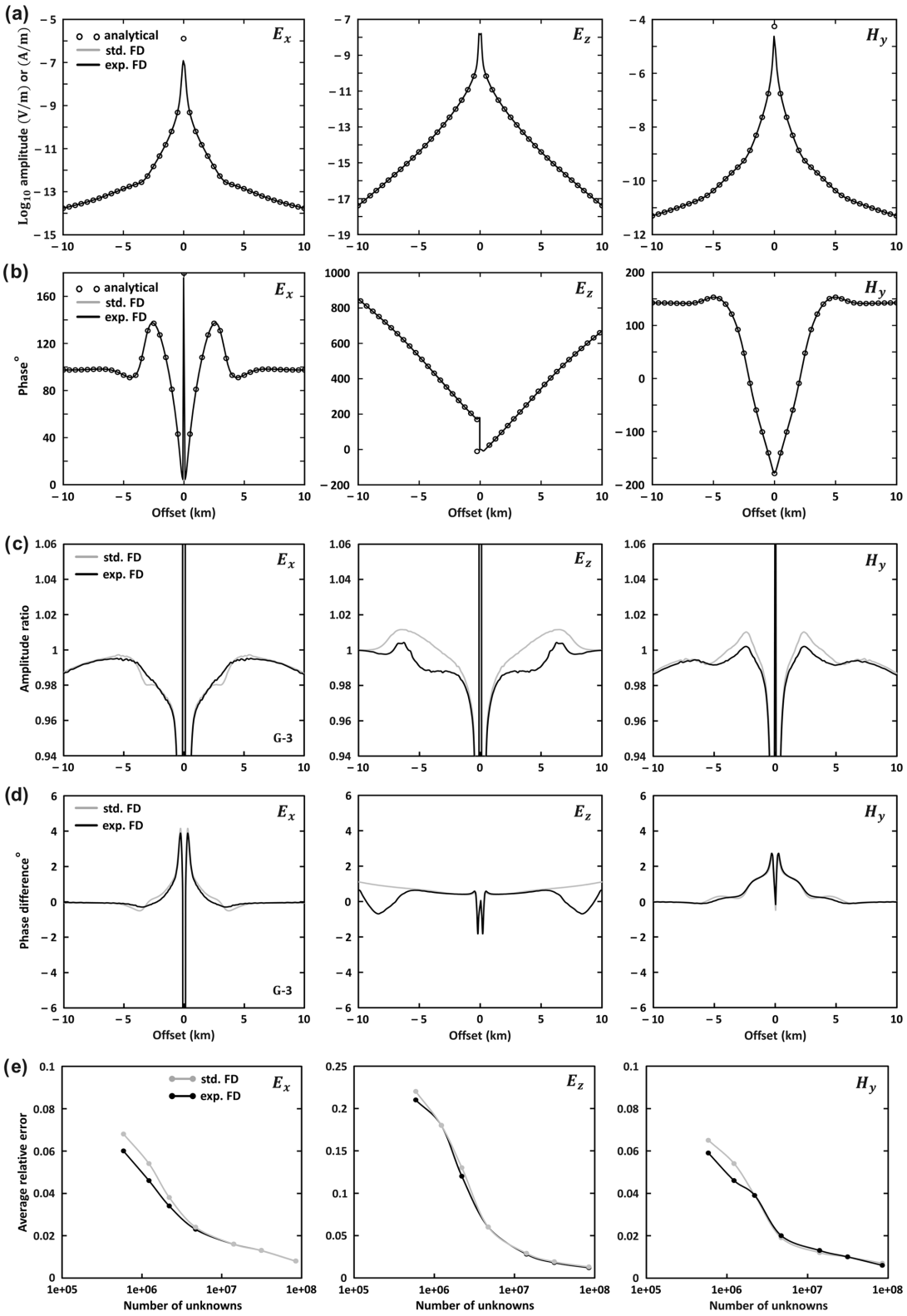

Figure 10. (a) Amplitude and (b) phase responses of E_x, E_z and H_y at 1 Hz for a shallow-water layered earth model built by removing 2.8 km of seawater from the deep-water model of Fig. 4. They are calculated using the standard (grey curve) and exponential (black curve) FD methods, as well as the plane-layer modelling (circles). (c) Normalized amplitude and (d) phase difference for the fields in (a) and (b) computed on a coarse grid G-3. (e) Average relative error plots for E_x, E_z and H_y as a function of the number of unknowns.

Table 6. The same as Table 5 but for the intermediate water depth model with 500 m of seawater.

		Matrix assembly time (s)		Number of iterations		Linear system solution time (s)	
Grids	Number of unknowns	Std. FD	Exp. FD	Std. FD	Exp. FD	Std. FD	Exp. FD
G-1	84 934 656	224.5	346.3	34	34	16100.2	16128.1
G-2	31 457 280	49.5	101.1	22	24	4259.4	4540.7
G-3	14 155 776	10.3	54.1	18	19	1535.8	1557.2
G-4	4 718 592	1.8	15.3	12	12	357.7	358.4
G-5	2 211 840	0.8	7.2	11	12	156.4	172.1
G-6	1 228 800	0.5	4.0	10	10	76.0	75.7
G-7	589 824	0.3	1.6	12	12	37.2	36.9

Accuracy improvements for upgoing field

We observed that the exponential FD method gave more accurate results as compared to the standard FD method for the deep-water cases, while the two were competitive for the shallow and intermediate water cases; this was illustrated by considering the total electric field. The behaviour for the latter cases can be explained by considering two facts related to the airwave. First, in shallow and intermediate water, the airwave contribution is usually stronger than the subsurface response at intermediate-to-long offsets (Constable & Weiss 2006; Nordskag & Amundsen 2007; Weidelt 2007; Andréis & MacGregor 2008). Second, as shown in Appendix B, the exponential FD approximation tends to standard FD approximation in the limit when conductivity tends to zero (e.g. in the air layer). Therefore, both these FD methods give very similar results for the airwave, which usually dominates the EM fields at intermediate-to-long offsets recorded at the seabed in the shallow and intermediate water cases. However, the situation is different if we consider only the upgoing component of the field, obtained using up-down decomposition (Amundsen *et al*. 2006; Nordskag & Amundsen 2007), and disregard the downgoing airwave. For the upgoing field, the exponential FD method gives more accurate results also for the shallow and intermediate cases. In the following paragraphs, we present up-down decomposition in brief followed by accuracy comparison of both FD methods for the upgoing electric field in the shallow and intermediate water cases.

The main purpose of acquiring CSEM data is to analyse the subsurface response, which has useful information about the subsurface (formation and/or hydrocarbon reservoir) resistivities. Therefore, a key requirement for CSEM modelling is to have a numerical method that gives superior accuracy specifically for the subsurface response. We use the fact that up-down decomposition of EM fields can be performed in order to separate upgoing and downgoing fields following Amundsen *et al*. (2006) and Nordskag & Amundsen (2007). They further demonstrate that the scattered fields (subsurface response) are mainly associated with upgoing fields. According to them, the upgoing electric field E_x^U for an inline configuration is given as

$$E_x^U(\mathbf{r}_r) = \frac{1}{2}\left[E_x(\mathbf{r}_r) - Z_f H_y(\mathbf{r}_r)\right], \tag{39}$$

where $E_x(\mathbf{r}_r)$ and $H_y(\mathbf{r}_r)$ are, respectively, the measured electric and magnetic fields at the receiver locations $\mathbf{r}_r$. For up-down decomposition below the seabed, Z_f is the characteristic impedance for the top formation immediately below the seabed. The characteristic impedance for a VTI medium is given by Mittet & Gabrielsen (2013) as

$$Z_f = \sqrt{-\mathrm{i}\mu\omega\rho_H}, \tag{40}$$

where ρ_H is the horizontal resistivity of the top formation immediately below the seabed. The motive of doing this decomposition is to remove the downgoing airwave and extract the upgoing electric field; this leaves signal carrying information mostly about the subsurface.

We first consider the previous shallow-water model example and compute the upgoing electric field using eqs (39) and (40). Fig. 12(a) shows the amplitude and phase responses of the upgoing electric field E_x^U computed for the shallow-water model. In this computation, we used E_x and H_y calculated with the standard FD, exponential FD, and plane-layer modelling methods. The normalized amplitudes and phase differences for E_x^U between results obtained with the plane-layer method, and results obtained via the standard and exponential FD methods are shown in Figs 12(b) and (c), respectively, for grids G-3 and G-4. These figures show that the numerical errors in the exponential FD method are smaller than those in the standard FD method.

We compute the relative errors, averaged over all of the inline offsets from −10 to 10 km, in the upgoing field E_x^U calculated using both methods. These, for the standard and exponential FD methods, are respectively 2.3 and 1.3 per cent on grid G-3; and 4.9 and 2.4 per cent on grid G-4. Fig. 13 shows a plot of average relative errors for E_x^U as a function of the number of unknowns for both methods. Except for the finest grid G-1 (with ∼85 million unknowns), we observe that the accuracy in the exponential FD method results is approximately two times better than in the corresponding standard FD method results. Here $\alpha = 7 \times 10^{-16}$ V m^{-1} was chosen to calculate average relative errors in E_x^U using eq. (38). This value was obtained using $\alpha = \frac{1}{2}\sqrt{(\alpha_E^2 + |Z_f|^2\alpha_H^2)}$, where α_E and α_H are respectively the ambient noise level in the electric and magnetic fields (see Table 3), with the assumption that the ambient noise sources in the electric and magnetic fields are uncorrelated. Note that if these noise sources are correlated, which can happen, for example in the case of MT noise, the resulting noise level in the upgoing field will be lower—the value of α we obtained is hence an upper bound. For reference, we also computed the average relative errors using the same value of α as in the deep-water layered earth model example for the electric field (see Table 3). This can be

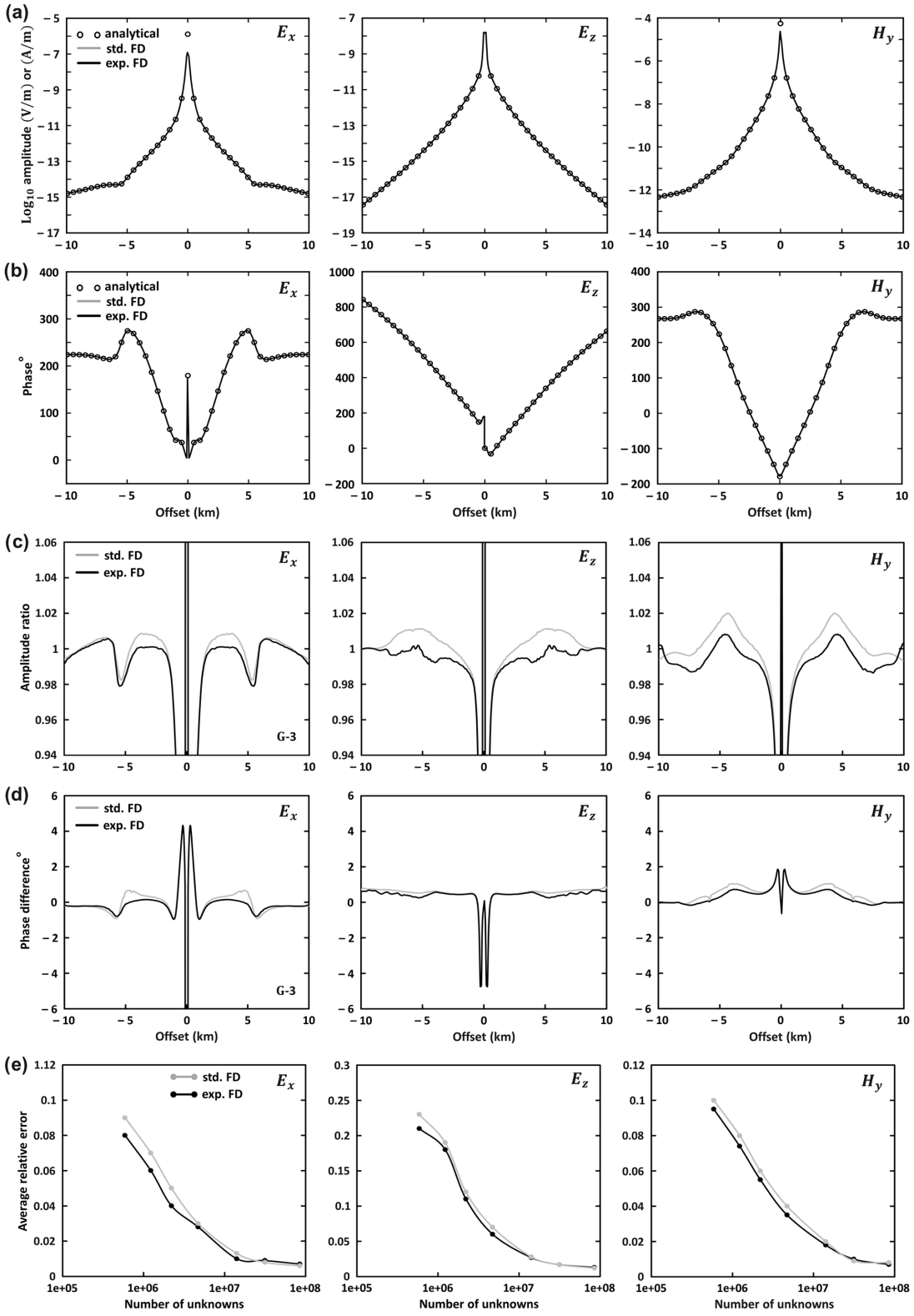

Figure 11. (a) Amplitude and (b) phase responses of E_x, E_z and H_y at 1 Hz for an intermediate water depth layered earth model built by removing 2.5 km of seawater from the deep-water model of Fig. 4. They are calculated using the standard (grey curve) and exponential (black curve) FD methods, as well as the plane-layer modelling (circles). (c) Normalized amplitude and (d) phase difference for the fields in (a) and (b) computed on a coarse grid G-3. (e) Average relative error plots for E_x, E_z and H_y as a function of the number of unknowns.

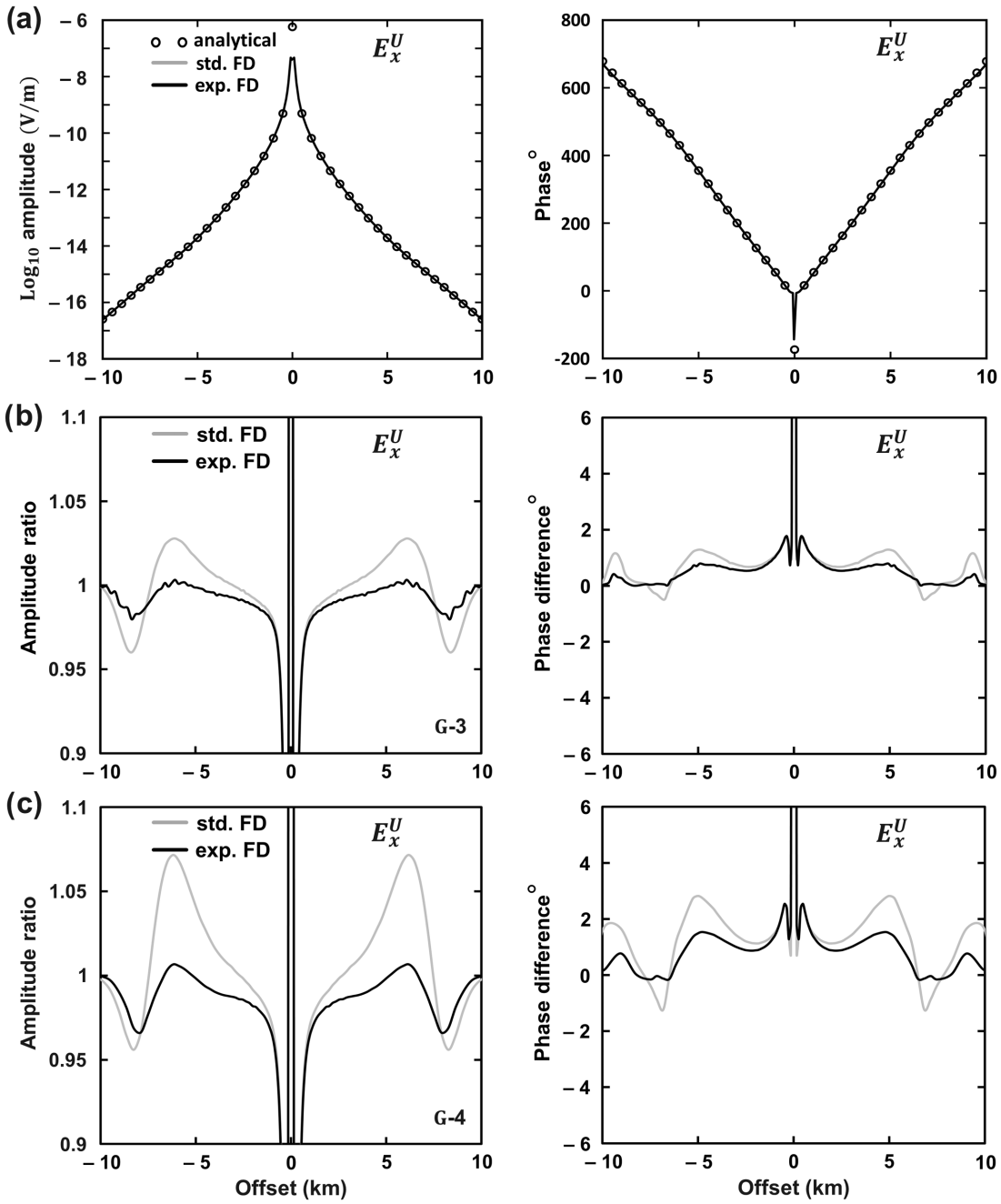

Figure 12. (a) Amplitude (left) and phase (right) responses for the upgoing electric field E_x^U obtained with E_x and H_y in Figs 10(a) and (b) using eqs (39) and (40). The grey curve, black curve and circles show E_x^U responses computed, respectively, with the standard FD, exponential FD and plane-layer modelling methods. Normalized amplitude (left) and phase difference (right) for E_x^U are shown in (b) for a coarse grid G-3. (c) Similar plots as (b), but for even coarser grid G-4.

considered a lower bound in the ambient noise level. The pattern we found was very similar to that in Fig. 13. Hence, the exponential FD gives more accurate results for the upgoing fields for the range of noise levels that can be considered relevant.

Fig. 13 indicates that the standard and exponential FD methods require, respectively, about 4.7 and 1.5 million unknowns to compute E_x^U with 5 per cent maximum allowed average relative error (see blue lines in Fig. 13). The corresponding modelling times would be about 565 and 145 s, respectively, for the standard and exponential FD methods. If the maximum allowed average relative error is 3 per cent then the standard and exponential FD methods require, respectively, 10 million and 3.4 million unknowns (see red lines in Fig. 13) or modelling times of respectively 2020 and 340 s. These modelling times were interpolated using Table 5 in combination with Fig. 13. This analysis shows that the exponential FD method requires about three times fewer unknowns or four to six times shorter modelling times as compared to standard FD method for the same accuracy.

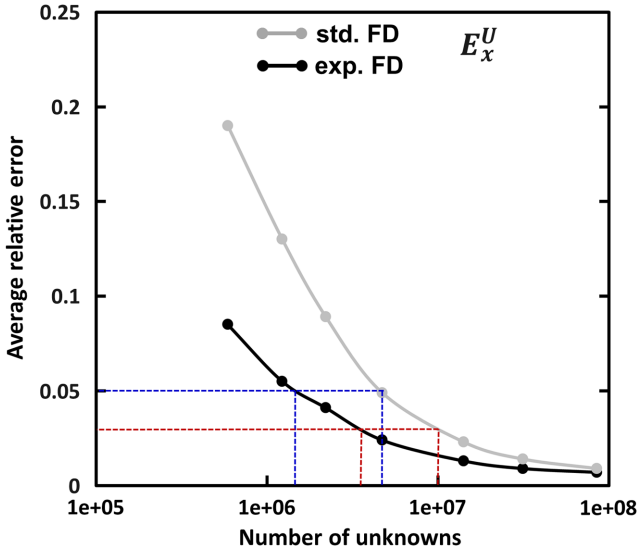

Figure 13. Average relative errors in the upgoing electric field E_x^U computed for a shallow-water CSEM model using the standard and exponential FD methods. Different number of unknowns correspond to seven different grids defined in Table 1. The errors are computed from the data plotted in Fig. 12(a) for grid G-3 and similar data for other grids and averaging them over offsets.

We now consider the intermediate water model example and compute the upgoing electric field using eqs (39) and (40). The amplitude and phase responses for the upgoing electric field E_x^U computed using E_x and H_y are shown in Fig. 14(a). The normalized amplitudes and phase differences for E_x^U between results obtained with the plane-layer method, and results obtained via the standard and exponential FD methods are shown in Figs 14(b) and (c), respectively, for coarse grids G-3 and G-4. It is clear from Figs 14(b) and (c) that the exponential FD method gives more accurate results than the standard FD method. Here $\alpha = 1.4 \times 10^{-15}$ V m^{-1} was chosen to compute the average relative error in the calculated upgoing field E_x^U; this value was obtained using α_E and α_H (see Table 3) as in the previous shallow-water layered earth example. The average relative errors for E_x^U calculated using the standard and exponential FD methods are, respectively, 2.0 per cent and 0.9 per cent on grid G-3 and 4.9 per cent and 2 per cent on grid G-4. Fig. 15 shows a plot of average relative errors for E_x^U as a function of the number of unknowns for the standard and exponential FD methods. Except for the finest grid G-1, the average relative errors in the exponential FD method results are nearly 2–2.5 times smaller than in the corresponding standard FD method results. In addition, we also computed the average relative errors with the same value of α as in the deep-water layered earth model example for the electric field (see Table 3) and found a very similar pattern as in Fig. 15.

In this case, the analysis using Fig. 15 shows that the standard and exponential FD methods require, respectively, about 4.6 and 1.5 million unknowns to compute E_x^U with 5 per cent maximum allowed average relative error (see blue lines in Fig. 15). The corresponding modelling times would be about 345 and 110 s, respectively, for the standard and exponential FD methods. For a 3 per cent maximum allowed average relative error, the standard and exponential FD methods require, respectively, 8.9 and 2.8 million unknowns (see red lines in Fig. 15) or modelling times of respectively 880 and 215 s. These modelling times were interpolated using Table 6 in combination with Fig. 15. It is clear that the exponential FD method requires about three times less unknowns or three to four times shorter modelling times as compared to standard FD method for the same accuracy in the upgoing fields.

CONCLUSIONS

We have presented a novel numerical scheme to perform 3-D EM simulations using an exponential FD method. To approximate the EM fields between grid nodes, the method employs exponential basis functions of the form $\{1, \exp[\pm(\nu_x x + \nu_y y + \nu_z z)]\}$ instead of low-degree polynomials as in the standard FD method. Since the EM fields have oscillatory and exponentially decaying behaviour in a conducting medium, the exponential FD method approximates them better between the nodes and thus provides more accurate results as compared to the standard FD method on a given grid. For a deep-water CSEM scenario, the observed improvement in the accuracy of computed EM fields is two to three times. Correspondingly, to achieve the same modelling accuracy, the exponential method requires two to six times fewer unknowns and 1.5 to 6 times shorter modelling times as compared to the standard method. For shallow-water and intermediate water depth models, the method mainly improves the accuracy for the upgoing fields. The accuracy for the downgoing fields is similar with both methods because in shallow and intermediate water these fields travel mostly through the highly resistive air layer where the exponents ν_x, ν_y and ν_z tend to zero and both FD methods become equivalent. For the upgoing electric field, the exponential FD method provides 2–2.5 times improvement in the accuracy, or, equivalently, three times fewer unknowns and three- to six-fold speed-up compared to the standard FD method that needs a finer grid to reach the same accuracy.

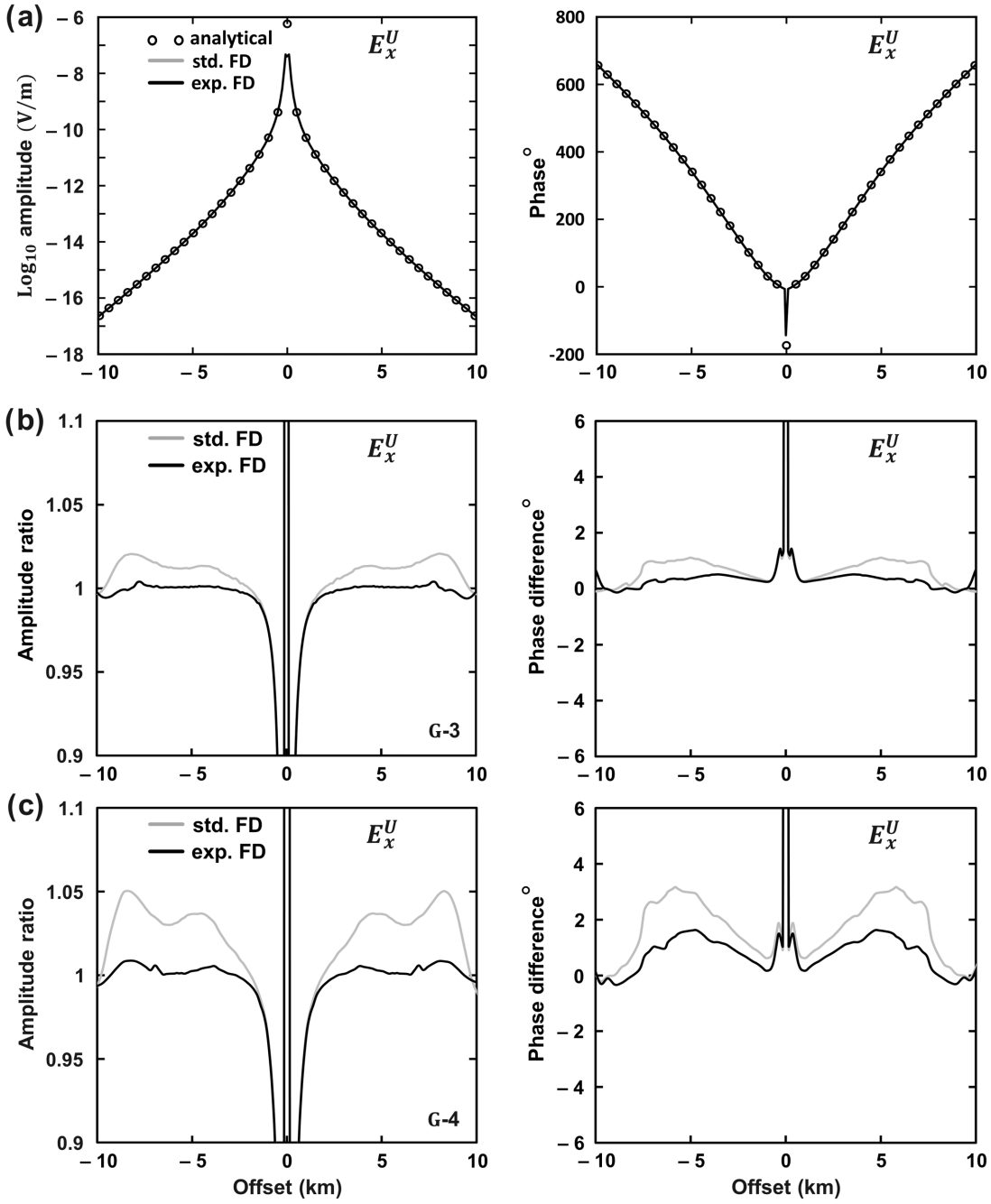

Figure 14. (a) Amplitude (left-hand side) and phase (right-hand side) responses for the upgoing electric field E_x^U obtained using E_x and H_y in Figs 11(a) and (b). The grey curve, black curve and circles show E_x^U responses computed, respectively, with the standard FD, exponential FD and plane-layer modelling methods. (b) Normalized amplitude (left-hand side) and phase difference (right-hand side) for E_x^U computed on a coarse grid G-3. (c) Similar plots as (b), but for even coarser grid G-4.

ACKNOWLEDGEMENTS

We thank EMGS for giving permission to publish the results and the Research Council of Norway for supporting this work through Petromaks program. We sincerely thank Dr Pravin Kumar Gupta for many constructive discussions on exponential fitting. We also express our gratitude to Dr Anders Malthe-Sørenssen and Dr Joakim Bergli for helpful and inspiring suggestions. The authors would like to thank Dr Mark Everett, Dr Sofia Davydycheva and an anonymous reviewer for their helpful suggestions and constructive comments.

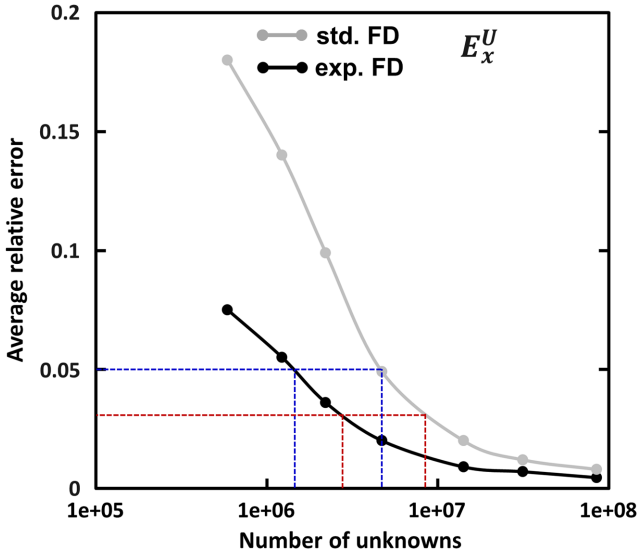

Figure 15. Plot of average relative errors for E_x^U as a function of the number of unknowns for an intermediate water depth CSEM model. These errors are computed from the data plotted in Fig. 14(a) for grid G-3 and similar data for other grids and averaging them over offsets.

REFERENCES

Amundsen, L., Løseth, L., Mittet, R., Ellingsrud, S. & Ursin, B., 2006. Decomposition of electromagnetic fields into upgoing and downgoing components, *Geophysics,* **71**(5), G211–G223.

Andréis, D. & MacGregor, L.M., 2008. Controlled-source electromagnetic sounding in shallow water: principles and applications, *Geophysics,* **73**(1), F21–F32.

Avdeev, D.B., 2005. Three-dimensional electromagnetic modelling and inversion from theory to application, *Surv. Geophys.,* **26,** 767–799.

Börner, R.-U., 2010. Numerical modeling in geo-electromagnetics: advances and challenges, *Surv. Geophys.,* **31,** 225–245.

Cole, J.B. & Banerjee, S., 2003. Applications of nonstandard finite difference models to computational electromagnetics, *J. Differ. Equ. Appl.,* **9**(12), 1099–1112.

Constable, S. & Weiss, C.J., 2006. Mapping thin resistors and hydrocarbons with marine EM methods: insights from 1D modeling, *Geophysics,* **71**(2), G43–G51.

da Silva, N.V., Morgan, J.V., Macgregor, L. & Warner, M., 2012. A finite element multifrontal method for 3D CSEM modeling in the frequency-domain, *Geophysics,* **77**(2), E101–E115.

Davydycheva, S., Druskin, V. & Habashy, T., 2003. An efficient finite-difference scheme for electromagnetic logging in 3D anisotropic inhomogeneous media, *Geophysics,* **68**(5), 1525–1536.

Ferziger, J.H. & Perić, M., 2002. *Computational Methods for Fluid Dynamics,* Springer.

Holberg, O., 1987. Computational aspects of the choice of operator and sampling interval for numerical differentiation in large-scale simulation of wave phenomena, *Geophys. Prospect.,* **35,** 629–655.

Ixaru, L.Gr., 1997. Operations on oscillatory functions, *Comput. Phys. Commun.,* **105,** 1–19.

Ixaru, L.Gr. & Berghe, G.V., 2004. *Exponential Fitting,* Kluwer Academic Publishers.

Jaysaval, P., 2012. Two-dimensional magnetotelluric modelling of earth using exponential finite difference method, *Master thesis,* Indian Institute of Technology Roorkee, Roorkee, India.

Jaysaval, P., Shantsev, D. & de la Kethulle de Ryhove, S., 2014. Fast multimodel finite-difference controlled-source electromagnetic simulations based on a Schur complement approach, *Geophysics,* **79**(6), E315–E327.

Lynch, D.R., 2005. *Numerical Partial Differential Equations for Environmental Scientists and Engineers: A First Practical Course,* Springer.

Løseth, L.O. & Ursin, B., 2007. Electromagnetic fields in planarly layered anisotropic media, *Geophys. J. Int.,* **170,** 44–80.

Mickens, R.E. (ed.), 2000. *Applications of Nonstandard Finite Difference Schemes,* World Scientific Publishing.

Mickens, R.E. (ed.), 2005. *Advances in the Applications of Nonstandard Finite Difference Schemes,* World Scientific Publishing.

Mittet, R., 2010. High-order finite-difference simulation of marine CSEM survey using a corresponding principle for wave and diffusion fields, *Geophysics,* **75**(1), F33–F50.

Mittet, R. & Gabrielsen, P.T., 2013. Decomposition in upgoing and downgoing fields and inversion of marine CSEM data, *Geophysics,* **78**(1), E1–E17.

Mittet, R. & Morten, J.P., 2013. The marine controlled-source electromagnetic method in shallow water, *Geophysics,* **78**(2), E67–E77.

Monk, P. & Süli, E., 1994. A convergence analysis of Yee's scheme on nonuniform grids, *SIAM J. Numer. Anal.,* **31**(2), 393–412.

Mulder, W.A., 2006. A multigrid solver for 3D electromagnetic diffusion, *Geophys. Prospect.,* **54,** 633–649.

Newman, G.A. & Alumbaugh, D.L., 1995. Frequency-domain modeling of airborne electromagnetic responses using staggered finite differences, *Geophys. Prospect.,* **43,** 1021–1042.

Nordskag, J.I. & Amundsen, L., 2007. Asymptotic airwave modeling for marine controlled-source electromagnetic surveying, *Geophysics,* **72**(6), F249–F255.

Patidar, K.C., 2005. On the use of nonstandard finite difference methods, *J. Differ. Equ. Appl.,* **11**(8), 735–758.

Ray, S., 2011. Simulation of electromagnetic response of layered earth using exponential finite difference method, *Master thesis,* Indian Institute of Technology Roorkee, Roorkee, India.

Shantsev, D.V. & Maaø, F.A., 2015. Rigorous interpolation near tilted interfaces in 3-D finite-difference EM modelling, *Geophys. J. Int.,* **200**(2), 745–757.

Streich, R., 2009. 3D finite-difference frequency-domain modeling of controlled-source electromagnetic data: direct solution and optimization for high accuracy, *Geophysics,* **74**(5), F95–F105.

Symes, W.W., Terentyev, I.S. & Vdovina, T.W., 2008. Gridding requirements for accurate finite difference simulation, in *Proceedings of the 78th SEG Annual International Meeting,* Las Vegas, USA, pp. 2077–2080.

Taflove, A. & Hagness, S.C., 2005. *Computational Electrodynamics: The Finite-Difference Time Domain Method,* 3rd edn, Artech House.

van der Vorst, H.A., 1992. BI-CGSTAB: a fast and smoothly converging variant of bi-CG for the solution of nonsymmetric linear systems, *SIAM J. Sci. Stat. Comput.,* **13,** 631–644.

Ward, S.H. & Hohmann, G.W., 1988. Electromagnetic theory for geophysical applications, in *Electromagnetic Methods in Applied Geophysics,* Vol. 1: Theory, pp. 131–311, ed. Nabighian, M.N., Society of Exploration Geophysicists.

Weidelt, P., 2007. Guided waves in marine CSEM, *Geophys. J. Int.,* **171,** 153–176.

Yee, K., 1966. Numerical solution of initial boundary value problems involving Maxwell's equations in isotropic media, *IEEE Trans. Antennas Propag.,* **14,** 302–307.

Zhdanov, M.S., 2009. *Geophysical Electromagnetic Theory and Methods,* Elsevier.

APPENDIX A: DERIVATION OF EXPONENTIAL FINITE-DIFFERENCE APPROXIMATION

The derivation of the exponential FD approximation of $\partial_y^2 E_x(\mathbf{r})$, $\partial_x E_y(\mathbf{r})$ and $\partial_y E_y(\mathbf{r})$ at $(x_i + \frac{\Delta x_i}{2},\ y_j,\ z_k)$ on the Yee staggered grid (Fig. 1) is summarized in this appendix. Consider the definition of operator $\mathcal{L}_{2y}[\Delta y_{j-1}, \Delta y_j, \mathbf{a}]$ in eq. (14)

$$\mathcal{L}_{2y}\left[\Delta y_{j-1}, \Delta y_j, \mathbf{a}\right] E_x(\mathbf{r}) = \left.\frac{\partial^2 E_x(x,y,z)}{\partial y^2}\right|_{i+\frac{1}{2},j,k} - \frac{1}{\Delta y_{j-1}\Delta y_j}\left[a_1 E^x_{i+\frac{1}{2},j+1,k} + a_2 E^x_{i+\frac{1}{2},j,k} + a_3 E^x_{i+\frac{1}{2},j-1,k}\right]. \tag{A1}$$

In exponential FDs, the field $E_x(\mathbf{r})$ between the nodal points is considered as some combination of exponential basis functions $\{1, \exp[\pm(\nu_x x + \nu_y y + \nu_z z)]\}$. Application of operator $\mathcal{L}_{2y}[\Delta y_{j-1}, \Delta y_j, \mathbf{a}]$ to the basis functions $\{1, \exp[\pm(\nu_x x + \nu_y y + \nu_z z)]\}$ yields

$$\mathcal{L}_{2y}\left[\Delta y_{j-1}, \Delta y_j, \mathbf{a}\right] 1 = -\frac{1}{\Delta y_{j-1}\Delta y_j}\left[a_1 + a_2 + a_3\right], \tag{A2}$$

$$\begin{aligned}
&\mathcal{L}_{2y}\left[\Delta y_{j-1}, \Delta y_j, \mathbf{a}\right] \exp\left\{\pm\left(\nu_x x + \nu_y y + \nu_z z\right)\right\} \\
&\quad = \nu_y^2 \exp\left\{\pm\left(\nu_x x + \nu_y y + \nu_z z\right)\right\}\Big|_{i+\frac{1}{2},j,k} \\
&\quad\quad - \frac{1}{\Delta y_{j-1}\Delta y_j}\left[a_1 \exp\left(\pm\left\{\nu_x\left(x_i + \frac{\Delta x_i}{2}\right) + \nu_y\left(y_j + \Delta y_j\right) + \nu_z z_k\right\}\right)\right. \\
&\quad\quad + a_2 \exp\left(\pm\left\{\nu_x\left(x_i + \frac{\Delta x_i}{2}\right) + \nu_y y_j + \nu_z z_k\right\}\right) \\
&\quad\quad \left. + a_3 \exp\left(\pm\left\{\nu_x\left(x_i + \frac{\Delta x_i}{2}\right) + \nu_y\left(y_j - \Delta y_{j-1}\right) + \nu_z z_k\right\}\right)\right]
\end{aligned} \tag{A3}$$

$$= \frac{\exp\left(\pm\left\{\nu_x\left(x_i + \frac{\Delta x_i}{2}\right) + \nu_y y_j + \nu_z z_k\right\}\right)}{\Delta y_{j-1}\Delta y_j}\left[\nu_y^2 \Delta y_{j-1}\Delta y_j - a_1 \exp\left(\pm\nu_y \Delta y_j\right) - a_2 - a_3 \exp\left(\mp\nu_y \Delta y_{j-1}\right)\right]. \tag{A4}$$

This can be written as

$$\mathcal{L}_{2y}\left[\Delta y_{j-1}, \Delta y_j, \mathbf{a}\right] \exp\left\{\pm\left(\nu_x x + \nu_y y + \nu_z z\right)\right\} = \frac{\exp\left(\pm\left\{\nu_x\left(x_i + \frac{\Delta x_i}{2}\right) + \nu_y y_j + \nu_z z_k\right\}\right)}{\Delta y_{j-1}\Delta y_j}\varepsilon^{\pm}_{2y}\left[\Delta y_{j-1}, \Delta y_j, \mathbf{a}\right], \tag{A5}$$

where

$$\varepsilon^{+}_{2y}\left[\Delta y_{j-1}, \Delta y_j, \mathbf{a}\right] = \nu_y^2 \Delta y_{j-1}\Delta y_j - a_1 \exp\left(\nu_y \Delta y_j\right) - a_2 - a_3 \exp\left(-\nu_y \Delta y_{j-1}\right), \tag{A6}$$

$$\varepsilon^{-}_{2y}\left[\Delta y_{j-1}, \Delta y_j, \mathbf{a}\right] = \nu_y^2 \Delta y_{j-1}\Delta y_j - a_1 \exp\left(-\nu_y \Delta y_j\right) - a_2 - a_3 \exp\left(\nu_y \Delta y_{j-1}\right). \tag{A7}$$

We construct the quantities $G^{\pm}_{2y}[\Delta y_{j-1}, \Delta y_j,\ \mathbf{a}]$ using $\varepsilon^{\pm}_{2y}[\Delta y_{j-1}, \Delta y_j, \mathbf{a}]$ as

$$G^{+}_{2y}\left[\Delta y_{j-1}, \Delta y_j, \mathbf{a}\right] = \frac{1}{2}\left[\varepsilon^{+}_{2y}\left(\Delta y_{j-1}, \Delta y_j, \mathbf{a}\right) + \varepsilon^{-}_{2y}\left(\Delta y_{j-1}, \Delta y_j, \mathbf{a}\right)\right] \tag{A8}$$

$$= \nu_y^2 \Delta y_{j-1}\Delta y_j - a_1 \eta_{-1}\left(\nu_y \Delta y_j\right) - a_2 - a_3 \eta_{-1}\left(\nu_y \Delta y_{j-1}\right), \tag{A9}$$

where $\eta_{-1}(\nu_y \Delta y) = \frac{1}{2}[\exp(\nu_y \Delta y) + \exp(-\nu_y \Delta y)]$.

Similarly,

$$G_{2y}^{-}\left[\Delta y_{j-1},\Delta y_j,\ \mathbf{a}\right]=\frac{1}{2v_y\sqrt{\Delta y_{j-1}\Delta y_j}}\left[\varepsilon_{2y}^{+}\left(\Delta y_{j-1},\Delta y_j,\ \mathbf{a}\right)-\varepsilon_{2y}^{-}\left(\Delta y_{j-1},\Delta y_j,\ \mathbf{a}\right)\right] \tag{A10}$$

$$=-a_1\sqrt{\frac{\Delta y_j}{\Delta y_{j-1}}}\eta_0\left(v_y\Delta y_j\right)+a_3\sqrt{\frac{\Delta y_{j-1}}{\Delta y_j}}\eta_0\left(v_y\Delta y_{j-1}\right), \tag{A11}$$

where $\eta_0(v_y\Delta y)=\frac{1}{2v_y\Delta y}[\exp(v_y\Delta y)-\exp(-v_y\Delta y)]$.

After constructing the expressions for $G_{2y}^{\pm}[\Delta y_{j-1},\Delta y_j,\mathbf{a}]$, our task is to find values for the set of coefficients $\mathbf{a}$. This can be done by setting $\mathcal{L}_{2y}[\Delta y_{j-1},\Delta y_j,\mathbf{a}]1=0$ and $\mathcal{L}_{2y}[\Delta y_{j-1},\Delta y_j,\mathbf{a}]\exp\{\pm(v_xx+v_yy+v_zz)\}=0$. Eqs (A5), (A8) and (A10) imply that $\mathcal{L}_{2y}[\Delta y_{j-1},\Delta y_j,\mathbf{a}]\exp\{\pm(v_xx+v_yy+v_zz)\}=0$ is equivalent to $G_{2y}^{\pm}[\Delta y_{j-1},\Delta y_j,\mathbf{a}]=0$. Therefore, to obtain $\mathbf{a}$, we need to solve $\mathcal{L}_{2y}[\Delta y_{j-1},\Delta y_j,\mathbf{a}]1=0$ and $G_{2y}^{\pm}[\Delta y_{j-1},\Delta y_j,\mathbf{a}]=0$. The solutions to these three equations yield the coefficients

$$a_1=\frac{v_y^2\Delta y_{j-1}\Delta y_j}{\left[\left\{\eta_{-1}\left(v_y\Delta y_j\right)-1\right\}+\left\{\eta_{-1}\left(v_y\Delta y_{j-1}\right)-1\right\}\frac{\Delta y_j}{\Delta y_{j-1}}\frac{\eta_0\left(v_y\Delta y_j\right)}{\eta_0\left(v_y\Delta y_{j-1}\right)}\right]}, \tag{A12}$$

$$a_3=\frac{\Delta y_j}{\Delta y_{j-1}}\frac{\eta_0\left(v_y\Delta y_j\right)}{\eta_0\left(v_y\Delta y_{j-1}\right)}a_1, \tag{A13}$$

$$a_2=-a_1-a_3. \tag{A14}$$

Now consider the exponential FD approximation of $\partial_xE_y(\mathbf{r})$ at $(x_i+\frac{\Delta x_i}{2},\ y_j,\ z_k)$ on the staggered grid

$$\left.\frac{\partial E_y\left(x,y,z\right)}{\partial x}\right|_{i+\frac{1}{2},j,k}\approx\frac{1}{\Delta x_i}\left\{b_1E_{i+1,j,k}^{y}+b_2E_{i,j,k}^{y}\right\}, \tag{A15}$$

where $\mathbf{b}\equiv[b_1,b_2]$ is a set of coefficients to be determined using exponential FD approximation. Define an operator $\mathcal{L}_{1x}[\Delta x_i,\mathbf{b}]$ such that

$$\mathcal{L}_{1x}\left[\Delta x_i,\mathbf{b}\right]E_y\left(\mathbf{r}\right)=\left.\frac{\partial E_y\left(x,y,z\right)}{\partial x}\right|_{i+\frac{1}{2},j,k}-\frac{1}{\Delta x_i}\left\{b_1E_{i+1,j,k}^{y}+b_2E_{i,j,k}^{y}\right\}. \tag{A16}$$

Following the above procedure, we apply the operator $\mathcal{L}_{1x}[\Delta x_i,\mathbf{b}]$ to the basis functions $\exp\{\pm(v_xx+v_yy+v_yz)\}$.

$$\begin{aligned}&\mathcal{L}_{1x}\left[\Delta y_i,\mathbf{b}\right]\exp\left\{\pm\left(v_xx+v_yy+v_zz\right)\right\}\\&\quad=\pm v_x\exp\left\{\pm\left(v_xx+v_yy+v_zz\right)\right\}\Big|_{i+\frac{1}{2},j,k}-\frac{1}{\Delta x_i}\left[b_1\exp\left(\pm\left\{v_x\left(x_i+\Delta x_i\right)+v_yy_j+v_zz_k\right\}\right)\right.\\&\qquad\left.+b_2\exp\left(\pm\left\{v_xx_i+v_yy_j+v_zz_k\right\}\right)\right]\end{aligned} \tag{A17}$$

$$=\frac{\exp\left(\pm\left\{v_x\left(x_i+\frac{\Delta x_i}{2}\right)+v_yy_j+v_zz_k\right\}\right)}{\Delta x_i}\left[\pm v_x\Delta x_i-b_1\exp\left(\pm v_x\frac{\Delta x_i}{2}\right)-b_2\exp\left(\mp v_x\frac{\Delta x_i}{2}\right)\right]. \tag{A18}$$

This can be written

$$\mathcal{L}_{1x}\left[\Delta x_i,\mathbf{b}\right]\exp\left\{\pm v\left(x+y+z\right)\right\}=\frac{\exp\left(\pm\left\{v_x\left(x_i+\frac{\Delta x_i}{2}\right)+v_yy_j+v_zz_k\right\}\right)}{\Delta x_i}\varepsilon_{1x}^{\pm}\left[\Delta x_i,\mathbf{b}\right], \tag{A19}$$

where

$$\varepsilon_{1x}^{+}\left[\Delta x_i,\mathbf{b}\right]=v_x\Delta x_i-b_1\exp\left(v_x\frac{\Delta x_i}{2}\right)-b_2\exp\left(-v_x\frac{\Delta x_i}{2}\right), \tag{A20}$$

$$\varepsilon_{1x}^{-}\left[\Delta x_i,\mathbf{b}\right]=-v_x\Delta x_i-b_1\exp\left(-v_x\frac{\Delta x_i}{2}\right)-b_2\exp\left(v_x\frac{\Delta x_i}{2}\right). \tag{A21}$$

We then construct $G_{1x}^{\pm}[\Delta x_i,\mathbf{b}]$ using $\varepsilon_{1x}^{\pm}[\Delta x_i,\mathbf{b}]$ as

$$G_{1x}^{+}\left[\Delta x_i,\mathbf{b}\right]=\frac{1}{2}\left[\varepsilon_{1x}^{+}\left(\Delta x_i,\mathbf{b}\right)+\varepsilon_{1x}^{-}\left(\Delta x_i,\mathbf{b}\right)\right] \tag{A22}$$

$$=-b_1\eta_{-1}\left(v_x\frac{\Delta x_i}{2}\right)-b_2\eta_{-1}\left(v_x\frac{\Delta x_i}{2}\right), \tag{A23}$$

$$G_{1x}^{-}\left[\Delta x_i, \mathbf{b}\right] = \frac{1}{\nu_x \Delta x_i}\left[\varepsilon_{1x}^{+}\left(\Delta x_i, \mathbf{b}\right) - \varepsilon_{1x}^{-}\left(\Delta x_i, \mathbf{b}\right)\right] \tag{A24}$$

$$= 2 - b_1\eta_0\left(\nu_x\frac{\Delta x_i}{2}\right) + b_2\eta_0\left(\nu_x\frac{\Delta x_i}{2}\right). \tag{A25}$$

Solving $G_{1x}^{\pm}[\Delta x_i, \mathbf{b}] = 0$ yields

$$b_1 = -b_2 = \frac{1}{\eta_0\left(\nu_x\frac{\Delta x_i}{2}\right)}. \tag{A26}$$

Finally, consider

$$\left.\frac{\partial E_y\left(x, y, z\right)}{\partial y}\right|_{i+\frac{1}{2},j,k} \approx \frac{1}{\Delta y_{sj}}\left\{c_1 E^{y}_{i+\frac{1}{2},j+\frac{1}{2},k} + c_2 E^{y}_{i+\frac{1}{2},j-\frac{1}{2},k}\right\}, \tag{A27}$$

where $\Delta y_{sj} = \frac{1}{2}(\Delta y_{j-1} + \Delta y_j)$, and $\mathbf{c} \equiv [c_1, c_2]$ is a set of coefficients to be determined for exponential FD approximation. Let us define the operator

$$\mathcal{L}_{1y}\left[\Delta y_{j-1}, \Delta y_j, \mathbf{c}\right] E_y\left(\mathbf{r}\right) = \left.\frac{\partial E_y\left(x, y, z\right)}{\partial y}\right|_{i+\frac{1}{2},j,k} - \frac{1}{\Delta y_{sj}}\left\{c_1 E^{y}_{i+\frac{1}{2},j+\frac{1}{2},k} + c_2 E^{y}_{i+\frac{1}{2},j-\frac{1}{2},k}\right\}. \tag{A28}$$

Applying this operator to the basis functions $\exp\{\pm(\nu_x x + \nu_y y + \nu_y z)\}$ gives

$$\begin{aligned}\mathcal{L}_{1y}&\left[\Delta y_{j-1}, \Delta y_j, \mathbf{c}\right]\exp\left\{\pm\left(\nu_x x + \nu_y y + \nu_z z\right)\right\}\\ &= \pm\nu_y \exp\left\{\pm\left(\nu_x x + \nu_y y + \nu_z z\right)\right\}\Big|_{i+\frac{1}{2},j,k} - \frac{1}{\Delta y_{sj}}\left[c_1\exp\left(\pm\left\{\nu_x\left(x_i + \frac{\Delta x_i}{2}\right) + \nu_y\left(y_j + \frac{\Delta y_j}{2}\right) + \nu_z z_k\right\}\right)\right.\\ &\left. + c_2\exp\left(\pm\left\{\nu_x\left(x_i + \frac{\Delta x_i}{2}\right) + \nu_y\left(y_j - \frac{\Delta y_{j-1}}{2}\right) + \nu_z z_k\right\}\right)\right]\end{aligned} \tag{A29}$$

$$= \frac{\exp\left(\pm\left\{\nu_x\left(x_i + \frac{\Delta x_i}{2}\right) + \nu_y y_j + \nu_z z_k\right\}\right)}{\Delta y_{sj}}\left[\pm\nu_y\Delta y_{sj} - c_1\exp\left(\pm\nu_y\frac{\Delta y_j}{2}\right) - c_2\exp\left(\mp\nu_y\frac{\Delta y_{j-1}}{2}\right)\right]. \tag{A30}$$

Let

$$\mathcal{L}_{1y}\left[\Delta y_{j-1}, \Delta y_j, \mathbf{c}\right]\exp\left\{\pm\left(\nu_x x + \nu_y y + \nu_z z\right)\right\} = \frac{\exp\left(\pm\left\{\nu_x\left(x_i + \frac{\Delta x_i}{2}\right) + \nu_y y_j + \nu_z z_k\right\}\right)}{\Delta y_{sj}}\varepsilon_{1y}^{\pm}\left[\Delta y_{j-1}, \Delta y_j,\ \mathbf{c}\right], \tag{A31}$$

where

$$\varepsilon_{1y}^{+}\left[\Delta y_{j-1}, \Delta y_j, \mathbf{c}\right] = \nu_y\Delta y_{sj} - c_1\exp\left(\nu_y\frac{\Delta y_j}{2}\right) - c_2\exp\left(-\nu_y\frac{\Delta y_{j-1}}{2}\right), \tag{A32}$$

$$\varepsilon_{1y}^{-}\left[\Delta y_{j-1}, \Delta y_j, \mathbf{c}\right] = -\nu_y\Delta y_{sj} - c_1\exp\left(-\nu_y\frac{\Delta y_j}{2}\right) - c_2\exp\left(\nu_y\frac{\Delta y_{j-1}}{2}\right). \tag{A33}$$

We construct $G_{1y}^{\pm}[\Delta y_{j-1}, \Delta y_j,\ \mathbf{c}]$ as

$$G_{1y}^{+}\left[\Delta y_{j-1}, \Delta y_j, \mathbf{c}\right] = \frac{1}{2}\left[\varepsilon_{1y}^{+}\left(\Delta y_{j-1}, \Delta y_j, \mathbf{c}\right) + \varepsilon_{1y}^{-}\left(\Delta y_{j-1}, \Delta y_j, \mathbf{c}\right)\right] \tag{A34}$$

$$= -c_1\eta_{-1}\left(\nu_y\frac{\Delta y_j}{2}\right) - c_2\eta_{-1}\left(\nu_y\frac{\Delta y_{j-1}}{2}\right), \tag{A35}$$

$$G_{1y}^{-}\left[\Delta y_{j-1}, \Delta y_j, \mathbf{c}\right] = \frac{1}{\nu_y\sqrt{\Delta y_j\Delta y_{j-1}}}\left[\varepsilon_{1y}^{+}\left(\Delta y_{j-1}, \Delta y_j, \mathbf{c}\right) - \varepsilon_{1y}^{-}\left(\Delta y_{j-1}, \Delta y_j, \mathbf{c}\right)\right] \tag{A36}$$

$$= \frac{2\Delta y_{sj}}{\sqrt{\Delta y_j\Delta y_{j-1}}} - \sqrt{\frac{\Delta y_j}{\Delta y_{j-1}}}c_1\eta_0\left(\nu_y\frac{\Delta y_j}{2}\right) + \sqrt{\frac{\Delta y_{j-1}}{\Delta y_j}}c_1\eta_0\left(\nu_y\frac{\Delta y_{j-1}}{2}\right). \tag{A37}$$

Solving $G^{\pm}_{1y}[\Delta y_{j-1}, \Delta y_j, \mathbf{c}] = 0$, we obtain

$$c_1 = \frac{2\Delta y_{sj}}{\left[\Delta y_j \eta_0\left(\nu_y \frac{\Delta y_j}{2}\right) + \Delta y_{j-1}\eta_0\left(\nu_y \frac{\Delta y_{j-1}}{2}\right)\frac{\eta_{-1}\left(\nu_y \frac{\Delta y_j}{2}\right)}{\eta_{-1}\left(\nu_y \frac{\Delta y_{j-1}}{2}\right)}\right]}, \tag{A38}$$

$$c_2 = -\frac{\eta_{-1}\left(\nu_y \frac{\Delta y_j}{2}\right)}{\eta_{-1}\left(\nu_y \frac{\Delta y_{j-1}}{2}\right)} c_1. \tag{A39}$$

APPENDIX B: LIMITING CASE OF EXPONENTIAL FINITE-DIFFERENCE APPROXIMATION

In our study, the values of the exponents, based on the frequency and node conductivity, are chosen as $\upsilon = \pm(-1+\mathrm{i})\sqrt{\frac{\mu\omega\sigma}{2}}$. This implies that υ tends to zero if either the conductivity σ or the frequency f tends to zero. In this appendix, we examine the behaviour of exponential FD approximation in the limit when ν_x, ν_y and $\nu_z \to 0$.

Let us consider the limiting cases for $\eta_0(\nu_y\Delta y)$, $\eta_{-1}(\nu_y\Delta y)$, $\frac{\eta_0(\nu_y\Delta y_j)}{\eta_0(\nu_y\Delta y_{j-1})}$ and $\frac{\eta_{-1}(\nu_y\frac{\Delta y_j}{2})}{\eta_{-1}(\nu_y\frac{\Delta y_{j-1}}{2})}$ when $\nu_y \to 0$.

$$\lim_{\nu_y\to 0}\eta_0\left(\nu_y\Delta y\right) = \lim_{\nu_y\to 0}\frac{1}{2\nu_y\Delta y}\left[\exp\left(\nu_y\Delta y\right) - \exp\left(-\nu_y\Delta y\right)\right]. \tag{B1}$$

Eq. (B1) being an indeterminate $\frac{0}{0}$ form, we apply l'Hôpital's rule, which gives

$$\lim_{\nu_y\to 0}\eta_0\left(\nu_y\Delta y\right) = 1. \tag{B2}$$

$$\lim_{\nu_y\to 0}\eta_{-1}\left(\nu_y\Delta y\right) = \lim_{\nu_y\to 0}\frac{1}{2}\left[\exp\left(\nu_y\Delta y\right) + \exp\left(-\nu_y\Delta y\right)\right] = 1. \tag{B3}$$

$$\lim_{\nu_y\to 0}\frac{\eta_0\left(\nu_y\Delta y_j\right)}{\eta_0\left(\nu_y\Delta y_{j-1}\right)} = \frac{\lim\limits_{\nu_y\to 0}\eta_0\left(\nu_y\Delta y_j\right)}{\lim\limits_{\nu_y\to 0}\eta_0\left(\nu_y\Delta y_{j-1}\right)}. \tag{B4}$$

Using limiting result of eq. (B2)

$$\lim_{\nu_y\to 0}\frac{\eta_0\left(\nu_y\Delta y_j\right)}{\eta_0\left(\nu_y\Delta y_{j-1}\right)} = 1. \tag{B5}$$

$$\lim_{\nu_y\to 0}\frac{\eta_{-1}\left(\nu_y\Delta y_j\right)}{\eta_{-1}\left(\nu_y\Delta y_{j-1}\right)} = \frac{\lim\limits_{\nu_y\to 0}\eta_{-1}\left(\nu_y\Delta y_j\right)}{\lim\limits_{\nu_y\to 0}\eta_{-1}\left(\nu_y\Delta y_{j-1}\right)}. \tag{B6}$$

Using limiting result of eq. (B3)

$$\lim_{\nu_y\to 0}\frac{\eta_{-1}\left(\nu_y\Delta y_j\right)}{\eta_{-1}\left(\nu_y\Delta y_{j-1}\right)} = 1. \tag{B7}$$

We now consider the limiting case for the set of coefficients $\mathbf{a} \equiv [a_1, a_2, a_3]$

$$\lim_{\nu_y\to 0} a_1 = \lim_{\nu_y\to 0}\frac{\nu_y^2\Delta y_{j-1}\Delta y_j}{\left[\left\{\eta_{-1}\left(\nu_y\Delta y_j\right)-1\right\} + \left\{\eta_{-1}\left(\nu_y\Delta y_{j-1}\right)-1\right\}\frac{\Delta y_j}{\Delta y_{j-1}}\frac{\eta_0\left(\nu_y\Delta y_j\right)}{\eta_0\left(\nu_y\Delta y_{j-1}\right)}\right]}. \tag{B8}$$

Using limiting result of eq. (B5)

$$\lim_{\nu_y\to 0} a_1 = \lim_{\nu_y\to 0}\frac{\nu_y^2\Delta y_{j-1}\Delta y_j}{\left[\left\{\eta_{-1}\left(\nu_y\Delta y_j\right)-1\right\} + \left\{\eta_{-1}\left(\nu_y\Delta y_{j-1}\right)-1\right\}\frac{\Delta y_j}{\Delta y_{j-1}}\right]}. \tag{B9}$$

Eq. (B9) being an indeterminate $\frac{0}{0}$ form, we apply l'Hôpital's rule

$$\lim_{\nu_y\to 0} a_1 = \lim_{\nu_y\to 0}\frac{2\nu_y\Delta y_{j-1}\Delta y_j}{\left[\frac{d}{d\nu_y}\left\{\eta_{-1}\left(\nu_y\Delta y_j\right)-1\right\} + \frac{d}{d\nu_y}\left\{\eta_{-1}\left(\nu_y\Delta y_{j-1}\right)-1\right\}\frac{\Delta y_j}{\Delta y_{j-1}}\right]} \tag{B10}$$

$$= \lim_{\nu_y \to 0} \frac{4\nu_y \Delta y_{j-1}}{\left[\left\{\exp\left(\nu_y \Delta y_j\right) - \exp\left(-\nu_y \Delta y_j\right)\right\} + \left\{\exp\left(\nu_y \Delta y_{j-1}\right) - \exp\left(-\nu_y \Delta y_{j-1}\right)\right\}\right]}. \tag{B11}$$

Eq. (B11) being again an indeterminate $\frac{0}{0}$ form, we apply l'Hôpital's rule

$$= \lim_{\nu_y \to 0} \frac{4\Delta y_{j-1}}{\left[\Delta y_j \left\{\exp\left(\nu_y \Delta y_j\right) + \exp\left(-\nu_y \Delta y_j\right)\right\} + \Delta y_{j-1} \left\{\exp\left(\nu_y \Delta y_{j-1}\right) + \exp\left(-\nu_y \Delta y_{j-1}\right)\right\}\right]} \tag{B12}$$

$$\lim_{\nu_y \to 0} a_1 = \frac{\Delta y_{j-1}}{\Delta y_{sj}}. \tag{B13}$$

$$\lim_{\nu_y \to 0} a_3 = \lim_{\nu_y \to 0} \frac{\Delta y_j}{\Delta y_{j-1}} \frac{\eta_0\left(\nu_y \Delta y_j\right)}{\eta_0\left(\nu_y \Delta y_{j-1}\right)} a_1. \tag{B14}$$

Using the limiting results of eqs (B5) and (B13) gives

$$\lim_{\nu_y \to 0} a_3 = \frac{\Delta y_j}{\Delta y_{sj}}. \tag{B15}$$

$$\lim_{\nu_y \to 0} a_2 = \lim_{\nu_y \to 0} (-a_1 - a_3) = -2. \tag{B16}$$

We now consider the limiting case for the set of coefficients $\mathbf{b} \equiv [b_1, b_2]$ and $\mathbf{c} \equiv [c_1, c_2]$

$$\lim_{\nu_x \to 0} b_1 = -\lim_{\nu_x \to 0} b_2 = \lim_{\nu_x \to 0} \frac{1}{\eta_0\left(\nu_x \frac{\Delta x_i}{2}\right)}. \tag{B17}$$

Using the limiting result of eq. (B2) gives

$$\lim_{\nu_x \to 0} b_1 = -\lim_{\nu_x \to 0} b_2 = 1. \tag{B18}$$

$$\lim_{\nu_y \to 0} c_1 = \lim_{\nu_y \to 0} \frac{2\Delta y_{sj}}{\left[\Delta y_j \eta_0\left(\nu_y \frac{\Delta y_j}{2}\right) + \Delta y_{j-1} \eta_0\left(\nu_y \frac{\Delta y_{j-1}}{2}\right) \frac{\eta_{-1}\left(\nu_y \frac{\Delta y_j}{2}\right)}{\eta_{-1}\left(\nu_y \frac{\Delta y_{j-1}}{2}\right)}\right]}. \tag{B19}$$

Using the limiting results of eqs (B2) and (B7) gives

$$\lim_{\nu_y \to 0} c_1 = \lim_{\nu_y \to 0} \frac{2\Delta y_{sj}}{\left[\Delta y_j + \Delta y_{j-1}\right]} = 1. \tag{B20}$$

$$\lim_{\nu_y \to 0} c_2 = -\lim_{\nu_y \to 0} \frac{\eta_{-1}\left(\nu_y \frac{\Delta y_j}{2}\right)}{\eta_{-1}\left(\nu_y \frac{\Delta y_{j-1}}{2}\right)} c_1. \tag{B21}$$

Using the limiting results of eqs (B7) and (B20) gives

$$\lim_{\nu_y \to 0} c_2 = -1. \tag{B22}$$

Eqs (B13), (B15), (B16), (B20) and (B22) give values for the set of coefficients $\mathbf{a} \equiv [a_1, a_2, a_3]$ and $\mathbf{c} \equiv [c_1, c_2]$ in the limit $\nu_y \to 0$, and eq. (B18) gives the set of coefficients $\mathbf{b} \equiv [b_1, b_2]$ in the limit $\nu_x \to 0$; these are exactly the same as corresponding coefficients for the standard FD approximations in eqs (9) and (10). Similarly, we can show that the exponential FD approximations of all the other x, y, and z-derivatives tend to the standard FD, respectively, in the limit when ν_x, ν_y and $\nu_z \to 0$.

APPENDIX C: EXPONENTIAL FINITE-DIFFERENCE EQUATIONS

The staggered grid exponential FD approximations to the x-, y- and z-projections of eq. (5), that is eqs (6), (7) and (8), respectively read

$$\frac{2}{\Delta x_i \eta_0\left(\nu^x_{i+\frac{1}{2},j,k} \frac{\Delta x_i}{2}\right)\left[\Delta y_j \eta_0\left(\nu^y_{i+\frac{1}{2},j,k} \frac{\Delta y_j}{2}\right) + \Delta y_{j-1} \eta_0\left(\nu^y_{i+\frac{1}{2},j,k} \frac{\Delta y_{j-1}}{2}\right) \frac{\eta_{-1}\left(\nu^y_{i+\frac{1}{2},j,k} \frac{\Delta y_j}{2}\right)}{\eta_{-1}\left(\nu^y_{i+\frac{1}{2},j,k} \frac{\Delta y_{j-1}}{2}\right)}\right]}$$

$$\times\left[E^{y}_{i+1,j+\frac{1}{2},k}-\frac{\eta_{-1}\left(\nu^{y}_{i+\frac{1}{2},j,k}\frac{\Delta y_j}{2}\right)}{\eta_{-1}\left(\nu^{y}_{i+\frac{1}{2},j,k}\frac{\Delta y_{j-1}}{2}\right)}E^{y}_{i+1,j-\frac{1}{2},k}-E^{y}_{i,j+\frac{1}{2},k}+\frac{\eta_{-1}\left(\nu^{y}_{i+\frac{1}{2},j,k}\frac{\Delta y_j}{2}\right)}{\eta_{-1}\left(\nu^{y}_{i+\frac{1}{2},j,k}\frac{\Delta y_{j-1}}{2}\right)}E^{y}_{i,j-\frac{1}{2},k}\right]$$

$$-\frac{(\nu^{y})^{2}_{i+\frac{1}{2},j,k}}{\left[\left\{\eta_{-1}\left(\nu^{y}_{i+\frac{1}{2},j,k}\Delta y_j\right)-1\right\}+\left\{\eta_{-1}\left(\nu^{y}_{i+\frac{1}{2},j,k}\Delta y_{j-1}\right)-1\right\}\frac{\Delta y_j}{\Delta y_{j-1}}\frac{\eta_0\left(\nu^{y}_{i+\frac{1}{2},j,k}\Delta y_j\right)}{\eta_0\left(\nu^{y}_{i+\frac{1}{2},j,k}\Delta y_{j-1}\right)}\right]}$$

$$\times\left[E^{x}_{i+\frac{1}{2},j+1,k}-\left\{1+\frac{\Delta y_j}{\Delta y_{j-1}}\frac{\eta_0\left(\nu^{y}_{i+\frac{1}{2},j,k}\Delta y_j\right)}{\eta_0\left(\nu^{y}_{i+\frac{1}{2},j,k}\Delta y_{j-1}\right)}\right\}E^{x}_{i+\frac{1}{2},j,k}+\frac{\Delta y_j}{\Delta y_{j-1}}\frac{\eta_0\left(\nu^{y}_{i+\frac{1}{2},j,k}\Delta y_j\right)}{\eta_0\left(\nu^{y}_{i+\frac{1}{2},j,k}\Delta y_{j-1}\right)}E^{x}_{i+\frac{1}{2},j-1,k}\right]$$

$$-\frac{(\nu^{z})^{2}_{i+\frac{1}{2},j,k}}{\left[\left\{\eta_{-1}\left(\nu^{z}_{i+\frac{1}{2},j,k}\Delta z_k\right)-1\right\}+\left\{\eta_{-1}\left(\nu^{z}_{i+\frac{1}{2},j,k}\Delta z_{k-1}\right)-1\right\}\frac{\Delta z_k}{\Delta z_{k-1}}\frac{\eta_0\left(\nu^{z}_{i+\frac{1}{2},j,k}\Delta z_k\right)}{\eta_0\left(\nu^{z}_{i+\frac{1}{2},j,k}\Delta z_{k-1}\right)}\right]}$$

$$\times\left[E^{x}_{i+\frac{1}{2},j,k+1}-\left\{1+\frac{\Delta z_k}{\Delta z_{k-1}}\frac{\eta_0\left(\nu^{z}_{i+\frac{1}{2},j,k}\Delta z_k\right)}{\eta_0\left(\nu^{z}_{i+\frac{1}{2},j,k}\Delta z_{k-1}\right)}\right\}E^{x}_{i+\frac{1}{2},j,k}+\frac{\Delta z_k}{\Delta z_{k-1}}\frac{\eta_0\left(\nu^{z}_{i+\frac{1}{2},j,k}\Delta z_k\right)}{\eta_0\left(\nu^{z}_{i+\frac{1}{2},j,k}\Delta z_{k-1}\right)}E^{x}_{i+\frac{1}{2},j,k-1}\right]$$

$$+\frac{2}{\Delta x_i\eta_0\left(\nu^{x}_{i+\frac{1}{2},j,k}\frac{\Delta x_i}{2}\right)\left[\Delta z_k\eta_0\left(\nu^{z}_{i+\frac{1}{2},j,k}\frac{\Delta z_k}{2}\right)+\Delta z_{k-1}\eta_0\left(\nu^{z}_{i+\frac{1}{2},j,k}\frac{\Delta z_{k-1}}{2}\right)\frac{\eta_{-1}\left(\nu^{z}_{i+\frac{1}{2},j,k}\frac{\Delta z_k}{2}\right)}{\eta_{-1}\left(\nu^{z}_{i+\frac{1}{2},j,k}\frac{\Delta z_{k-1}}{2}\right)}\right]}$$

$$\times\left[E^{z}_{i+1,j,k+\frac{1}{2}}-\frac{\eta_{-1}\left(\nu^{z}_{i+\frac{1}{2},j,k}\frac{\Delta z_k}{2}\right)}{\eta_{-1}\left(\nu^{z}_{i+\frac{1}{2},j,k}\frac{\Delta z_{k-1}}{2}\right)}E^{z}_{i+1,j,k-\frac{1}{2}}-E^{z}_{i,j,k+\frac{1}{2}}+\frac{\eta_{-1}\left(\nu^{z}_{i+\frac{1}{2},j,k}\frac{\Delta z_k}{2}\right)}{\eta_{-1}\left(\nu^{z}_{i+\frac{1}{2},j,k}\frac{\Delta z_{k-1}}{2}\right)}E^{z}_{i,j,k-\frac{1}{2}}\right]-\mathrm{i}\omega\mu\tilde{\sigma}^{x}_{i+\frac{1}{2},j,k}E^{x}_{i+\frac{1}{2},j,k}=\mathrm{i}\omega\mu J^{x}_{i+\frac{1}{2},j,k},\quad\text{(C1)}$$

$$\frac{2}{\Delta y_j\eta_0\left(\nu^{y}_{i,j+\frac{1}{2},k}\frac{\Delta y_j}{2}\right)\left[\Delta z_k\eta_0\left(\nu^{z}_{i,j+\frac{1}{2},k}\frac{\Delta z_k}{2}\right)+\Delta z_{k-1}\eta_0\left(\nu^{z}_{i,j+\frac{1}{2},k}\frac{\Delta z_{k-1}}{2}\right)\frac{\eta_{-1}\left(\nu^{z}_{i,j+\frac{1}{2},k}\frac{\Delta z_k}{2}\right)}{\eta_{-1}\left(\nu^{z}_{i,j+\frac{1}{2},k}\frac{\Delta z_{k-1}}{2}\right)}\right]}$$

$$\times\left[E^{z}_{i,j+1,k+\frac{1}{2}}-\frac{\eta_{-1}\left(\nu^{z}_{i,j+\frac{1}{2},k}\frac{\Delta z_k}{2}\right)}{\eta_{-1}\left(\nu^{z}_{i,j+\frac{1}{2},k}\frac{\Delta z_{k-1}}{2}\right)}E^{z}_{i,j+1,k-\frac{1}{2}}-E^{z}_{i,j,k+\frac{1}{2}}+\frac{\eta_{-1}\left(\nu^{z}_{i,j+\frac{1}{2},k}\frac{\Delta z_k}{2}\right)}{\eta_{-1}\left(\nu^{z}_{i,j+\frac{1}{2},k}\frac{\Delta z_{k-1}}{2}\right)}E^{z}_{i,j,k-\frac{1}{2}}\right]$$

$$-\frac{(\nu^{z})^{2}_{i,j+\frac{1}{2},k}}{\left[\left\{\eta_{-1}\left(\nu^{z}_{i,j+\frac{1}{2},k}\Delta z_k\right)-1\right\}+\left\{\eta_{-1}\left(\nu^{z}_{i,j+\frac{1}{2},k}\Delta z_{k-1}\right)-1\right\}\frac{\Delta z_k}{\Delta z_{k-1}}\frac{\eta_0\left(\nu^{z}_{i,j+\frac{1}{2},k}\Delta z_k\right)}{\eta_0\left(\nu^{z}_{i,j+\frac{1}{2},k}\Delta z_{k-1}\right)}\right]}$$

$$\times\left[E^{y}_{i,j+\frac{1}{2},k+1}-\left\{1+\frac{\Delta z_k}{\Delta z_{k-1}}\frac{\eta_0\left(\nu^{z}_{i,j+\frac{1}{2},k}\Delta z_k\right)}{\eta_0\left(\nu^{z}_{i,j+\frac{1}{2},k}\Delta z_{k-1}\right)}\right\}E^{y}_{i,j+\frac{1}{2},k}+\frac{\Delta z_k}{\Delta z_{k-1}}\frac{\eta_0\left(\nu^{z}_{i,j+\frac{1}{2},k}\Delta z_k\right)}{\eta_0\left(\nu^{z}_{i,j+\frac{1}{2},k}\Delta z_{k-1}\right)}E^{y}_{i,j+\frac{1}{2},k-1}\right]$$

$$-\frac{(\nu^{x})^{2}_{i,j+\frac{1}{2},k}}{\left[\left\{\eta_{-1}\left(\nu^{x}_{i,j+\frac{1}{2},k}\Delta x_i\right)-1\right\}+\left\{\eta_{-1}\left(\nu^{x}_{i,j+\frac{1}{2},k}\Delta x_{i-1}\right)-1\right\}\frac{\Delta x_i}{\Delta x_{i-1}}\frac{\eta_0\left(\nu^{x}_{i,j+\frac{1}{2},k}\Delta x_i\right)}{\eta_0\left(\nu^{x}_{i,j+\frac{1}{2},k}\Delta x_{i-1}\right)}\right]}$$

$$\times\left[E^{y}_{i+1,j+\frac{1}{2},k}-\left\{1+\frac{\Delta x_i}{\Delta x_{i-1}}\frac{\eta_0\left(\nu^{x}_{i,j+\frac{1}{2},k}\Delta x_i\right)}{\eta_0\left(\nu^{x}_{i,j+\frac{1}{2},k}\Delta x_{i-1}\right)}\right\}E^{y}_{i,j+\frac{1}{2},k}+\frac{\Delta x_i}{\Delta x_{i-1}}\frac{\eta_0\left(\nu^{x}_{i,j+\frac{1}{2},k}\Delta x_i\right)}{\eta_0\left(\nu^{x}_{i,j+\frac{1}{2},k}\Delta x_{i-1}\right)}E^{y}_{i-1,j+\frac{1}{2},k}\right]$$

$$+\frac{2}{\Delta y_j\eta_0\left(\nu^{y}_{i,j+\frac{1}{2},k}\frac{\Delta y_j}{2}\right)\left[\Delta x_i\eta_0\left(\nu^{x}_{i,j+\frac{1}{2},k}\frac{\Delta x_i}{2}\right)+\Delta x_{i-1}\eta_0\left(\nu^{x}_{i,j+\frac{1}{2},k}\frac{\Delta x_{i-1}}{2}\right)\frac{\eta_{-1}\left(\nu^{x}_{i,j+\frac{1}{2},k}\frac{\Delta x_i}{2}\right)}{\eta_{-1}\left(\nu^{x}_{i,j+\frac{1}{2},k}\frac{\Delta x_{i-1}}{2}\right)}\right]}$$

$$\times\left[E^{x}_{i+\frac{1}{2},j+1,k}-\frac{\eta_{-1}\left(\nu^{x}_{i,j+\frac{1}{2},k}\frac{\Delta x_i}{2}\right)}{\eta_{-1}\left(\nu^{x}_{i,j+\frac{1}{2},k}\frac{\Delta x_{i-1}}{2}\right)}E^{x}_{i-\frac{1}{2},j+1,k}-E^{x}_{i+\frac{1}{2},j,k}+\frac{\eta_{-1}\left(\nu^{x}_{i,j+\frac{1}{2},k}\frac{\Delta x_i}{2}\right)}{\eta_{-1}\left(\nu^{x}_{i,j+\frac{1}{2},k}\frac{\Delta x_{i-1}}{2}\right)}E^{x}_{i-\frac{1}{2},j,k}\right]-\mathrm{i}\omega\mu\tilde{\sigma}^{y}_{i,j+\frac{1}{2},k}E^{y}_{i,j+\frac{1}{2},k}=\mathrm{i}\omega\mu J^{y}_{i,j+\frac{1}{2},k},\tag{C2}$$

$$\frac{2}{\Delta z_k\eta_0\left(\nu^{z}_{i,j,k+\frac{1}{2}}\frac{\Delta z_k}{2}\right)\left[\Delta x_i\eta_0\left(\nu^{x}_{i,j,k+\frac{1}{2}}\frac{\Delta x_i}{2}\right)+\Delta x_{i-1}\eta_0\left(\nu^{x}_{i,j,k+\frac{1}{2}}\frac{\Delta x_{i-1}}{2}\right)\frac{\eta_{-1}\left(\nu^{x}_{i,j,k+\frac{1}{2}}\frac{\Delta x_i}{2}\right)}{\eta_{-1}\left(\nu^{x}_{i,j,k+\frac{1}{2}}\frac{\Delta x_{i-1}}{2}\right)}\right]}$$

$$\times\left[E^{x}_{i+\frac{1}{2},j,k+1}-\frac{\eta_{-1}\left(\nu^{x}_{i,j,k+\frac{1}{2}}\frac{\Delta x_i}{2}\right)}{\eta_{-1}\left(\nu^{x}_{i,j,k+\frac{1}{2}}\frac{\Delta x_{i-1}}{2}\right)}E^{x}_{i-\frac{1}{2},j,k+1}-E^{x}_{i+\frac{1}{2},j,k}+\frac{\eta_{-1}\left(\nu^{x}_{i,j,k+\frac{1}{2}}\frac{\Delta x_i}{2}\right)}{\eta_{-1}\left(\nu^{x}_{i,j,k+\frac{1}{2}}\frac{\Delta x_{i-1}}{2}\right)}E^{x}_{i-\frac{1}{2},j,k}\right]$$

$$-\frac{(\nu^{x})^{2}_{i,j,k+\frac{1}{2}}}{\left[\left\{\eta_{-1}\left(\nu^{x}_{i,j,k+\frac{1}{2}}\Delta x_i\right)-1\right\}+\left\{\eta_{-1}\left(\nu^{x}_{i,j,k+\frac{1}{2}}\Delta x_{i-1}\right)-1\right\}\frac{\Delta x_i}{\Delta x_{i-1}}\frac{\eta_0\left(\nu^{x}_{i,j,k+\frac{1}{2}}\Delta x_i\right)}{\eta_0\left(\nu^{x}_{i,j,k+\frac{1}{2}}\Delta x_{i-1}\right)}\right]}$$

$$\times\left[E^{z}_{i+1,j,k+\frac{1}{2}}-\left\{1+\frac{\Delta x_i}{\Delta x_{i-1}}\frac{\eta_0\left(\nu^{x}_{i,j,k+\frac{1}{2}}\Delta x_i\right)}{\eta_0\left(\nu^{x}_{i,j,k+\frac{1}{2}}\Delta x_{i-1}\right)}\right\}E^{z}_{i,j,k+\frac{1}{2}}+\frac{\Delta x_i}{\Delta x_{i-1}}\frac{\eta_0\left(\nu^{x}_{i,j,k+\frac{1}{2}}\Delta x_i\right)}{\eta_0\left(\nu^{x}_{i,j,k+\frac{1}{2}}\Delta x_{i-1}\right)}E^{z}_{i-1,j,k+\frac{1}{2}}\right]$$

$$-\frac{(\nu^{y})^{2}_{i,j,k+\frac{1}{2}}}{\left[\left\{\eta_{-1}\left(\nu^{y}_{i,j,k+\frac{1}{2}}\Delta y_j\right)-1\right\}+\left\{\eta_{-1}\left(\nu^{y}_{i,j,k+\frac{1}{2}}\Delta y_{j-1}\right)-1\right\}\frac{\Delta y_j}{\Delta y_{j-1}}\frac{\eta_0\left(\nu^{y}_{i,j,k+\frac{1}{2}}\Delta y_j\right)}{\eta_0\left(\nu^{y}_{i,j,k+\frac{1}{2}}\Delta y_{j-1}\right)}\right]}$$

$$\times\left[E^{z}_{i,j+1,k+\frac{1}{2}}-\left\{1+\frac{\Delta y_j}{\Delta y_{j-1}}\frac{\eta_0\left(\nu^{y}_{i,j,k+\frac{1}{2}}\Delta y_j\right)}{\eta_0\left(\nu^{y}_{i,j,k+\frac{1}{2}}\Delta y_{j-1}\right)}\right\}E^{z}_{i,j,k+\frac{1}{2}}+\frac{\Delta y_j}{\Delta y_{j-1}}\frac{\eta_0\left(\nu^{y}_{i,j,k+\frac{1}{2}}\Delta y_j\right)}{\eta_0\left(\nu^{y}_{i,j,k+\frac{1}{2}}\Delta y_{j-1}\right)}E^{z}_{i,j-1,k+\frac{1}{2}}\right]$$

$$+\frac{2}{\Delta z_k\eta_0\left(\nu^{z}_{i,j,k+\frac{1}{2}}\frac{\Delta z_k}{2}\right)\left[\Delta y_j\eta_0\left(\nu^{y}_{i,j,k+\frac{1}{2}}\frac{\Delta y_j}{2}\right)+\Delta y_{j-1}\eta_0\left(\nu^{y}_{i,j,k+\frac{1}{2}}\frac{\Delta y_{j-1}}{2}\right)\frac{\eta_{-1}\left(\nu^{y}_{i,j,k+\frac{1}{2}}\frac{\Delta y_j}{2}\right)}{\eta_{-1}\left(\nu^{y}_{i,j,k+\frac{1}{2}}\frac{\Delta y_{j-1}}{2}\right)}\right]}$$

$$\times\left[E^{y}_{i,j+\frac{1}{2},k+1}-\frac{\eta_{-1}\left(\nu^{y}_{i,j,k+\frac{1}{2}}\frac{\Delta y_j}{2}\right)}{\eta_{-1}\left(\nu^{y}_{i,j,k+\frac{1}{2}}\frac{\Delta y_{j-1}}{2}\right)}E^{y}_{i,j-\frac{1}{2},k+1}-E^{y}_{i,j+\frac{1}{2},k}+\frac{\eta_{-1}\left(\nu^{y}_{i,j,k+\frac{1}{2}}\frac{\Delta y_j}{2}\right)}{\eta_{-1}\left(\nu^{y}_{i,j,k+\frac{1}{2}}\frac{\Delta y_{j-1}}{2}\right)}E^{y}_{i,j-\frac{1}{2},k}\right]-\mathrm{i}\omega\mu\tilde{\sigma}^{z}_{i,j,k+\frac{1}{2}}E^{z}_{i,j,k+\frac{1}{2}}=\mathrm{i}\omega\mu J^{z}_{i,j,k+\frac{1}{2}},\tag{C3}$$

where Δx_i, Δy_j and Δz_k are, respectively, the length, width and height of the grid cell with main node (x_i, y_j, z_k) located at the top left corner (Fig. 1); $\eta_{-1}(\nu_h\Delta h)=\frac{1}{2}[\exp(\nu_h\Delta h)+\exp(-\nu_h\Delta h)]$ and $\eta_0(\nu_h\Delta h)=\frac{1}{2\nu_h\Delta h}[\exp(\nu_h\Delta h)-\exp(-\nu_h\Delta h)]$ for $h=x$, y or z.

APPENDIX D: LEADING TERMS OF TRUNCATION ERROR

We first consider $\partial_y^2 E_x(\mathbf{r})$ and revisit the standard FD approximation by considering a set of monomials $\{1, xyz, x^2y^2z^2, x^3y^3z^3, \ldots\ldots\}$. Application of operator $\mathcal{L}_{2y}[\Delta y_{j-1}, \Delta y_j, \mathbf{a}]$ defined in eq. (14) to these monomials yields

$$\mathcal{L}_{2y}\left[\Delta y_{j-1}, \Delta y_j, \mathbf{a}\right] 1 = -\frac{1}{\Delta y_{j-1}\Delta y_j}\left[a_1 + a_2 + a_3\right], \tag{D1}$$

$$\mathcal{L}_{2y}\left[\Delta y_{j-1}, \Delta y_j, \mathbf{a}\right] xyz = -\frac{xyz}{\Delta y_{j-1}\Delta y_j}\left[a_1 + a_2 + a_3\right] - \frac{xz}{\Delta y_{j-1}\Delta y_j}\left[a_1\Delta y_j - a_3\Delta y_{j-1}\right], \tag{D2}$$

$$\begin{aligned}\mathcal{L}_{2y}&\left[\Delta y_{j-1}, \Delta y_j, \mathbf{a}\right] x^2y^2z^2 \\ &= -\frac{x^2y^2z^2}{\Delta y_{j-1}\Delta y_j}\left[a_1 + a_2 + a_3\right] - \frac{2yx^2z^2}{\Delta y_{j-1}\Delta y_j}\left[a_1\Delta y_j - a_3\Delta y_{j-1}\right] \\ &\quad - \frac{x^2z^2}{\Delta y_{j-1}\Delta y_j}\left[a_1{\Delta y_j}^2 + a_3{\Delta y_{j-1}}^2 - 2\Delta y_{j-1}\Delta y_j\right],\end{aligned} \tag{D3}$$

$$\begin{aligned}\mathcal{L}_{2y}&\left[\Delta y_{j-1}, \Delta y_j, \mathbf{a}\right] x^3y^3z^3 \\ &= -\frac{x^3y^3z^3}{\Delta y_{j-1}\Delta y_j}\left[a_1 + a_2 + a_3\right] - \frac{3y^2x^3z^3}{\Delta y_{j-1}\Delta y_j}\left[a_1\Delta y_j - a_3\Delta y_{j-1}\right] \\ &\quad - \frac{3yx^3z^3}{\Delta y_{j-1}\Delta y_j}\left[a_1{\Delta y_j}^2 + a_3{\Delta y_{j-1}}^2 - 2\Delta y_{j-1}\Delta y_j\right], \\ &\quad - \frac{x^3z^3}{\Delta y_{j-1}\Delta y_j}\left[a_1{\Delta y_j}^3 - a_3{\Delta y_{j-1}}^3\right],\end{aligned} \tag{D4}$$

$$\begin{aligned}\mathcal{L}_{2y}&\left[\Delta y_{j-1}, \Delta y_j, \mathbf{a}\right] x^4y^4z^4 \\ &= -\frac{x^4y^4z^4}{\Delta y_{j-1}\Delta y_j}\left[a_1 + a_2 + a_3\right] - \frac{4y^3x^4z^4}{\Delta y_{j-1}\Delta y_j}\left[a_1\Delta y_j - a_3\Delta y_{j-1}\right] \\ &\quad - \frac{6y^2x^4z^4}{\Delta y_{j-1}\Delta y_j}\left[a_1{\Delta y_j}^2 + a_3{\Delta y_{j-1}}^2 - 2\Delta y_{j-1}\Delta y_j\right], \\ &\quad - \frac{4yx^4z^4}{\Delta y_{j-1}\Delta y_j}\left[a_1{\Delta y_j}^3 - a_3{\Delta y_{j-1}}^3\right] - \frac{x^4z^4}{\Delta y_{j-1}\Delta y_j}\left[a_1{\Delta y_j}^4 + a_3{\Delta y_{j-1}}^4\right],\end{aligned} \tag{D5}$$

etc. at $x = x_i + \frac{\Delta x_i}{2}$, $y = y_j$ and $z = z_k$.

We can also compute $\mathcal{L}_{2y}[\Delta y_{j-1}, \Delta y_j, \mathbf{a}]x^m y^m z^m$, where $m = 0,\ 1,\ 2,\ 3, \ldots$, at $y = 0$ and denote them as $L_{2y}^m[\Delta y_{j-1}, \Delta y_j, \mathbf{a}]$. We have

$$L_{2y}^0\left[\Delta y_{j-1}, \Delta y_j, \mathbf{a}\right] = -\frac{1}{\Delta y_{j-1}\Delta y_j}\left[a_1 + a_2 + a_3\right], \tag{D6}$$

$$L_{2y}^1\left[\Delta y_{j-1}, \Delta y_j, \mathbf{a}\right] = -\frac{xz}{\Delta y_{j-1}\Delta y_j}\left[a_1\Delta y_j - a_3\Delta y_{j-1}\right], \tag{D7}$$

$$L_{2y}^2\left[\Delta y_{j-1}, \Delta y_j, \mathbf{a}\right] = -\frac{x^2z^2}{\Delta y_{j-1}\Delta y_j}\left[a_1{\Delta y_j}^2 + a_3{\Delta y_{j-1}}^2 - 2\Delta y_{j-1}\Delta y_j\right], \tag{D8}$$

and for $k = 2,\ 3,\ 4, \ldots\ldots$

$$L_{2y}^{2k-1}\left[\Delta y_{j-1}, \Delta y_j, \mathbf{a}\right] = -\frac{x^{2k-1}z^{2k-1}}{\Delta y_{j-1}\Delta y_j}\left[a_1{\Delta y_j}^{2k-1} - a_3{\Delta y_{j-1}}^{2k-1}\right], \tag{D9}$$

$$L_{2y}^{2k}\left[\Delta y_{j-1}, \Delta y_j, \mathbf{a}\right] = -\frac{x^{2k}z^{2k}}{\Delta y_{j-1}\Delta y_j}\left[a_1{\Delta y_j}^{2k} + a_3{\Delta y_{j-1}}^{2k}\right]. \tag{D10}$$

In the standard FD, the fields $E_x(\mathbf{r})$, $E_y(\mathbf{r})$ and $E_z(\mathbf{r})$ are taken as a linear combination of monomials, for example $E_x(\mathbf{r}) = e_0 + e_1xyz + e_2x^2y^2z^2 + \cdots$, with constants $e_0, e_1, e_2 \ldots$. Thus, we have

$$\mathcal{L}_{2y}\left[\Delta y_{j-1},\ \Delta y_j, \mathbf{a}\right] E_x(\mathbf{r}) = e_0\mathcal{L}_{2y}\left[\Delta y_{j-1}, \Delta y_j, \mathbf{a}\right] 1 + e_1\mathcal{L}_{2y}\left[\Delta y_{j-1}, \Delta y_j, \mathbf{a}\right] xyz + e_2\mathcal{L}_{2y}\left[\Delta y_{j-1}, \Delta y_j, \mathbf{a}\right] x^2y^2z^2 \ldots. \tag{D11}$$

Using the expressions for $\mathcal{L}_{2y}[\Delta y_{j-1}, \Delta y_j, \mathbf{a}]x^m y^m z^m$ for $m = 0,\ 1,\ 2, \ldots$ from eqs (D1) to (D5), and $L^m_{2y}[\Delta y_{j-1}, \Delta y_j, \mathbf{a}]$ from eqs (D6) to (D10) we have,

$$\begin{aligned}
&\mathcal{L}_{2y}\left[\Delta y_{j-1},\ \Delta y_j, \mathbf{a}\right] E_x(\mathbf{r}) \\
&= L^0_{2y}\left[\Delta y_{j-1}, \Delta y_j, \mathbf{a}\right]\left(e_0 + e_1 xyz + e_2 x^2y^2z^2 + e_3 x^3y^3z^3 + \cdots\right) \\
&\quad + L^1_{2y}\left[\Delta y_{j-1}, \Delta y_j, \mathbf{a}\right]\left(e_1 + 2e_2 xyz + 3e_3 x^2y^2z^2 + \cdots\right) \\
&\quad + L^2_{2y}\left[\Delta y_{j-1}, \Delta y_j, \mathbf{a}\right]\left(e_2 + 3e_3 xyz + 6e_4 x^2y^2z^2 + \cdots\right) + \cdots \qquad \text{(D12)} \\
&= L^0_{2y}\left[\Delta y_{j-1}, \Delta y_j, \mathbf{a}\right] E_x(\mathbf{r}) + \frac{1}{1!xz} L^1_{2y}\left[\Delta y_{j-1}, \Delta y_j, \mathbf{a}\right] \partial_y E_x(\mathbf{r}) \\
&\quad + \frac{1}{2!x^2z^2} L^2_{2y}\left[\Delta y_{j-1}, \Delta y_j, \mathbf{a}\right] \partial_y^2 E_x(\mathbf{r}) + \cdots \\
&\quad + \frac{1}{m!x^m z^m} L^m_{2y}\left[\Delta y_{j-1}, \Delta y_j, \mathbf{a}\right] \partial_y^m E_x(\mathbf{r}) + \cdots . \qquad \text{(D13)}
\end{aligned}$$

The set of coefficients $\mathbf{a}$ for the standard FD method is obtained by setting $\mathcal{L}_{2y}[\Delta y_{j-1}, \Delta y_j, \mathbf{a}]1 = 0$, $\mathcal{L}_{2y}[\Delta y_{j-1}, \Delta y_j, \mathbf{a}]xyz = 0$ and $\mathcal{L}_{2y}[\Delta y_{j-1}, \Delta y_j, \mathbf{a}]x^2y^2z^2 = 0$. Eqs (D1) and (D6) imply that $\mathcal{L}_{2y}[\Delta y_{j-1}, \Delta y_j, \mathbf{a}]1 = 0$ is equivalent to $L^0_{2y}[\Delta y_{j-1}, \Delta y_j, \mathbf{a}] = 0$; eqs (D1), (D2), (D6) and (D7) imply that the pair of conditions $\mathcal{L}_{2y}[\Delta y_{j-1}, \Delta y_j, \mathbf{a}]1 = 0$ and $\mathcal{L}_{2y}[\Delta y_{j-1}, \Delta y_j, \mathbf{a}]xyz = 0$ is equivalent to $L^0_{2y}[\Delta y_{j-1}, \Delta y_j, \mathbf{a}] = L^1_{2y}[\Delta y_{j-1}, \Delta y_j, \mathbf{a}] = 0$; and so on. Therefore, to obtain $\mathbf{a}$ for the standard FD, we need to solve $L^0_{2y}[\Delta y_{j-1}, \Delta y_j, \mathbf{a}] = 0$, $L^1_{2y}[\Delta y_{j-1}, \Delta y_j, \mathbf{a}] = 0$ and $L^2_{2y}[\Delta y_{j-1}, \Delta y_j, \mathbf{a}] = 0$. The solutions to these three equations yield the coefficients: $a_1 = \frac{\Delta y_{j-1}}{\Delta y_{sj}}$, $a_2 = -2$ and $a_3 = \frac{\Delta y_j}{\Delta y_{sj}}$. These are the same as the coefficients in eq. (9). Moreover, for these values, we notice that $L^k_{2y}[\Delta y_{j-1}, \Delta y_j, \mathbf{a}] \neq 0$ for $k = 3,\ 4,\ 5, \ldots$. Therefore, eq. (D13) implies

$$\mathcal{L}_{2y}\left[\Delta y_{j-1}, \Delta y_j, \mathbf{a}\right] E_x(\mathbf{r}) = \frac{1}{3!x^3z^3} L^3_{2y}\left[\Delta y_{j-1}, \Delta y_j, \mathbf{a}\right] \partial_y^3 E_x(\mathbf{r}) + \frac{1}{4!x^4z^4} L^4_{2y}\left[\Delta y_{j-1}, \Delta y_j, \mathbf{a}\right] \partial_y^4 E_x(\mathbf{r}) + \cdots . \qquad \text{(D14)}$$

Using eqs (D9) and (D10) in eq. (D14) and substituting the values of a_1 and a_3 for the standard FD approximation we get

$$\mathcal{L}_{2y}\left[\Delta y_{j-1}, \Delta y_j, \mathbf{a}\right] E_x(\mathbf{r}) = -\frac{1}{3}\left(\Delta y_j - \Delta y_{j-1}\right) \partial_y^3 E_x(\mathbf{r}) - \frac{1}{12}\left(\Delta {y_j}^2 + \Delta {y_{j-1}}^2 - \Delta y_j \Delta y_{j-1}\right) \partial_y^4 E_x(\mathbf{r}) + \cdots . \qquad \text{(D15)}$$

Therefore, the leading terms of the truncation error for the standard FD approximation are

$$\tau^{\text{std}}_{2y}(\mathbf{r}) = -\frac{1}{3}\left(\Delta y_j - \Delta y_{j-1}\right) \partial_y^3 E_x(\mathbf{r}) - \frac{1}{12}\left(\Delta {y_j}^2 + \Delta {y_{j-1}}^2 - \Delta y_j \Delta y_{j-1}\right) \partial_y^4 E_x(\mathbf{r}) . \qquad \text{(D16)}$$

It is important to note that the first leading term of the error contains a factor $\partial_y^3 E_x(\mathbf{r})$ and a PDE $\partial_y^3 E_x(\mathbf{r}) = 0$ is the one which has three independent solutions and their linear combination is of the form $E_x(\mathbf{r}) = \psi_1(x, z) + \psi_2(x, z)y + \psi_3(x, z)y^2$, where coefficients $\psi_1(x, z)$, $\psi_2(x, z)$ and $\psi_3(x, z)$ are some functions of variables x and z. For $\psi_1(x, z) = 1$, $\psi_2(x, z) = xz$ and $\psi_3(x, z) = x^2z^2$, the three linear independent solutions are $\{1,\ xyz, x^2y^2z^2\}$ which are the basis functions for the standard FD method. Moreover, if the cell size is uniform, that is $\Delta y_j = \Delta y_{j-1}$, the first leading term in eq. (D16) will be zero. We further notice that $L^3_{2y}[\Delta y_{j-1}, \Delta y_j, \mathbf{a}]$ will also be zero for a uniform grid. Therefore, we need to consider $\{1,\ xyz, x^2y^2z^2, x^3y^3z^3\}$ as the basis functions and hence a term with the factor $\partial_y^4 E_x(\mathbf{r})$ in the leading terms. A PDE $\partial_y^4 E_x(\mathbf{r}) = 0$ is now the one that has four independent solutions. These four solutions can be the new set of basis functions $\{1,\ xyz, x^2y^2z^2, x^3y^3z^3\}$.

In the exponential FD approximations, a PDE $(\partial_y^3 - \nu_y^2\partial_y)E_x(\mathbf{r}) = 0$ is the one which has three independent solutions that can be the exponential FD basis functions $\{1, \exp[\pm(\nu_x x + \nu_y y + \nu_z z)]\}$. Following the analogy of the standard FD approximations, the first leading term of the error in the exponential FD should be of the form

$$A_1\left(\partial_y^3 - \nu_y^2\partial_y\right) E_x(\mathbf{r}) . \qquad \text{(D17)}$$

The coefficient of $\partial_y E_x(\mathbf{r})$ should be the same in eqs (D13) and (D17), that is

$$A_1 = -\frac{1}{\nu_y^2 xz} L^1_{2y}\left[\Delta y_{j-1}, \Delta y_j, \mathbf{a}\right] = \frac{1}{\nu_y^2 \Delta y_{j-1}\Delta y_j}\left[a_1 \Delta y_j - a_3 \Delta y_{j-1}\right] . \qquad \text{(D18)}$$

Using the expression for a_1 and a_3 from eqs (15) and (16)

$$A_1 = -\Delta y_j \frac{\eta_0\left(\nu_y \Delta y_j\right) - \eta_0\left(\nu_y \Delta y_{j-1}\right)}{\eta_0\left(\nu_y \Delta y_{j-1}\right) Q\left(\nu_y, \Delta y_{j-1}, \Delta y_j\right)}, \qquad \text{(D19)}$$

where $Q(\nu_y, \Delta y_{j-1}, \Delta y_j) = \{\eta_{-1}(\nu_y \Delta y_j) - 1\} + \{\eta_{-1}(\nu_y \Delta y_{j-1}) - 1\} \frac{\Delta y_j}{\Delta y_{j-1}} \frac{\eta_0(\nu_y \Delta y_j)}{\eta_0(\nu_y \Delta y_{j-1})}$ with $\eta_{-1}(\nu_y \Delta y) = \frac{1}{2}[\exp(\nu_y \Delta y) + \exp(-\nu_y \Delta y)]$ and $\eta_0(\nu_y \Delta y) = \frac{1}{2\nu_y \Delta y}[\exp(\nu_y \Delta y) - \exp(-\nu_y \Delta y)]$.

If the grid is uniform, we need to consider a higher order term since $A_1 = 0$. Let if the set of basis functions for the exponential FD is $\{1, xyz, \exp[\pm(\nu_x x + \nu_y y + \nu_z z)]\}$, then a PDE $(\partial_y^4 - \nu_y^2\partial_y^2)E_x(\mathbf{r}) = 0$ has these basis functions as linear independent solutions. Therefore, the leading terms of the truncation error read

$$\tau_{2y}^{\exp}(\mathbf{r}) = A_1\left(\partial_y^3 - \nu_y^2\partial_y\right)E_x(\mathbf{r}) + A_2\left(\partial_y^4 - \nu_y^2\partial_y^2\right)E_x(\mathbf{r}), \tag{D20}$$

where A_1 is given in eq. (D19) and A_2 is obtained by comparing the coefficient of $\partial_y^2 E_x(\mathbf{r})$ in eqs (D13) and (D20). This comparison implies,

$$A_2 = -\frac{1}{2!\nu_y^2 x^2 z^2} L_{2y}^2\left[\Delta y_{j-1}, \Delta y_j, \mathbf{a}\right] = \frac{1}{2\nu_y^2 \Delta y_{j-1}\Delta y_j}\left[a_1 {\Delta y_j}^2 + a_3 {\Delta y_{j-1}}^2 - 2\Delta y_{j-1}\Delta y_j\right]. \tag{D21}$$

Using the expression for a_1 and a_3 from eqs (15) and (16)

$$A_2 = -\frac{1}{2\nu_y^2}\left[2 - \frac{\nu_y^2}{Q\left(\nu_y, \Delta y_{j-1}, \Delta y_j\right)}\left\{{\Delta y_j}^2 + \Delta y_{j-1}\Delta y_j \frac{\eta_0\left(\nu_y \Delta y_j\right)}{\eta_0\left(\nu_y \Delta y_{j-1}\right)}\right\}\right]. \tag{D22}$$

To obtain the leading terms of the error for FD approximation of $\partial_y\partial_x E_y(\mathbf{r})$, we first compute the leading terms of the error for $\frac{\partial E_y(x,y,z)}{\partial x}|_{i+\frac{1}{2},j,k}$ followed by one for $\frac{\partial E_y(x,y,z)}{\partial y}|_{i+\frac{1}{2},j,k}$ for both FD approximations.

Following the above procedure, we can easily show that the application of operators $\mathcal{L}_{1x}[\Delta x_i, \mathbf{b}]$ and $\mathcal{L}_{1y}[\Delta y_{j-1}, \Delta y_j, \mathbf{c}]$ on $E_y(\mathbf{r})$ with monomials as basis functions gives

$$\mathcal{L}_{1x}\left[\Delta x_i, \mathbf{b}\right]E_y(\mathbf{r}) = -\frac{1}{24}{\Delta x_i}^2\partial_x^3 E_y(\mathbf{r}) - \frac{1}{1920}{\Delta x_i}^4\partial_x^5 E_y(\mathbf{r}) + \cdots, \tag{D23}$$

$$\mathcal{L}_{1y}\left[\Delta y_{j-1}, \Delta y_j, \mathbf{c}\right]E_y(\mathbf{r}) = -\frac{1}{4}\left(\Delta y_j - \Delta y_{j-1}\right)\partial_y^2 E_y(\mathbf{r}) - \frac{1}{24}\left({\Delta y_j}^2 + {\Delta y_{j-1}}^2 - \Delta y_j\Delta y_{j-1}\right)\partial_y^3 E_y(\mathbf{r}) + \cdots. \tag{D24}$$

Therefore, the leading terms of the truncation error for the standard FD in approximating $\frac{\partial E_y(x,y,z)}{\partial x}|_{i+\frac{1}{2},j,k}$ and $\frac{\partial E_y(x,y,z)}{\partial y}|_{i+\frac{1}{2},j,k}$ are, respectively,

$$\tau_{1x}^{\text{std}}(\mathbf{r}) = -\frac{1}{24}{\Delta x_i}^2\partial_x^3 E_y(\mathbf{r}), \tag{D25}$$

$$\tau_{1y}^{\text{std}}(\mathbf{r}) = -\frac{1}{4}\left(\Delta y_j - \Delta y_{j-1}\right)\partial_y^2 E_y(\mathbf{r}) - \frac{1}{24}\left({\Delta y_j}^2 + {\Delta y_{j-1}}^2 - \Delta y_j\Delta y_{j-1}\right)\partial_y^3 E_y(\mathbf{r}). \tag{D26}$$

The corresponding leading terms of the error for the exponential FD are

$$\tau_{1x}^{\exp}(\mathbf{r}) = -\frac{1}{\nu_x^2}\left[\frac{\eta_0\left(\nu_x\frac{\Delta x_i}{2}\right) - 1}{\eta_0\left(\nu_x\frac{\Delta x_i}{2}\right)}\right]\left(\partial_x^3 - \nu_x^2\partial_x\right)E_y(\mathbf{r}), \tag{D27}$$

$$\tau_{1y}^{\exp}(\mathbf{r}) = C_1\left(\partial_y^2 - \nu_y^2\right)E_y(\mathbf{r}) + C_2\left(\partial_y^3 - \nu_y^2\partial_y\right)E_y(\mathbf{r}), \tag{D28}$$

where $C_1 = -\frac{2}{\nu_y^2 R(\nu_y, \Delta y_{j-1}, \Delta y_j)}\left[\frac{\eta_{-1}(\nu_y\frac{\Delta y_j}{2}) - \eta_{-1}(\nu_y\frac{\Delta y_{j-1}}{2})}{\eta_{-1}(\nu_y\frac{\Delta y_{j-1}}{2})}\right]$ and $C_2 = -\frac{1}{\nu_y^2}\left[1 - \frac{1}{R(\nu_y, \Delta y_j, \Delta y_{j-1})}\left\{\Delta y_j + \Delta y_{j-1}\frac{\eta_{-1}(\nu_y\frac{\Delta y_j}{2})}{\eta_{-1}(\nu_y\frac{\Delta y_{j-1}}{2})}\right\}\right]$, with $R(\nu_y, \Delta y_{j-1}, \Delta y_j)$ $= \Delta y_j\eta_0(\nu_y\frac{\Delta y_j}{2}) + \Delta y_{j-1}\eta_0(\nu_y\frac{\Delta y_{j-1}}{2})\frac{\eta_{-1}(\nu_y\frac{\Delta y_j}{2})}{\eta_{-1}(\nu_y\frac{\Delta y_{j-1}}{2})}$.

To compute the leading terms of the error in the mixed derivative $\partial_y\partial_x E_y(\mathbf{r})$, consider,

$$\left.\frac{\partial^2 E_y(x,y,z)}{\partial y\partial x}\right|_{i+\frac{1}{2},j,k} = \frac{\partial}{\partial y}\left[\frac{\partial E_y(x,y,z)}{\partial x}\right]_{i+\frac{1}{2},j,k} \tag{D29}$$

$$= \frac{\partial}{\partial y}\left[\frac{E_y(x+\Delta x_i, y, z) - E_y(x,y,z)}{\Delta x_i} + \tau_{1x}^{\text{std}}(x,y,z) + \cdots\right]_{i+\frac{1}{2},j,k} \tag{D30}$$

$$= \frac{1}{\Delta x_i}\left[\frac{E_y\left(x+\Delta x_i, y+\frac{\Delta y_j}{2}, z\right) - E_y\left(x+\Delta x_i, y-\frac{\Delta y_{j-1}}{2}, z\right)}{\Delta y_{sj}} + \tau_{1y}^{\text{std}}(x+\Delta x_i, y, z)\right.$$
$$\left. - \frac{E_y\left(x, y+\frac{\Delta y_j}{2}, z\right) - E_y\left(x, y-\frac{\Delta y_{j-1}}{2}, z\right)}{\Delta y_{sj}} - \tau_{1y}^{\text{std}}(x,y,z) + \cdots\right] + \partial_y\tau_{1x}^{\text{std}}(x,y,z) + \cdots \tag{D31}$$

$$= \left[\frac{E_y\left(x+\Delta x_i, y+\frac{\Delta y_j}{2}, z\right) - E_y\left(x+\Delta x_i, y-\frac{\Delta y_j}{2}, z\right) - E_y\left(x, y+\frac{\Delta y_j}{2}, z\right) + E_y\left(x, y-\frac{\Delta y_j}{2}, z\right)}{\Delta x_i \Delta y_{sj}} \right.$$

$$\left. + \partial_x \tau_{1y}^{\mathrm{std}}(x,y,z) + \partial_y \tau_{1x}^{\mathrm{std}}(x,y,z) + \cdots, \right. \tag{D32}$$

since $\partial_x \tau_{1y}^{\mathrm{std}}(x,y,z) = \{\tau_{1y}^{\mathrm{std}}(x+\Delta x_i, y, z) - \tau_{1y}^{\mathrm{std}}(x,y,z)\}/\Delta x_i$.

Therefore, the leading terms of the truncation error in approximating $\partial_y \partial_x E_y(\mathbf{r})$ with the standard FD are

$$\tau_{2xy}^{\mathrm{std}}(\mathbf{r}) = \partial_x \tau_{1y}^{\mathrm{std}}(\mathbf{r}) + \partial_y \tau_{1x}^{\mathrm{std}}(\mathbf{r}), \tag{D33}$$

where $\tau_{1x}^{\mathrm{std}}(\mathbf{r})$ and $\tau_{1y}^{\mathrm{std}}(\mathbf{r})$ are given in eqs (D25) and (D26), respectively.

Similarly, the leading terms of the truncation error in approximating $\partial_y \partial_x E_y(\mathbf{r})$ with the exponential FD are

$$\tau_{2xy}^{\mathrm{exp}}(\mathbf{r}) = \partial_x \tau_{1y}^{\mathrm{exp}}(\mathbf{r}) + \partial_y \tau_{1x}^{\mathrm{exp}}(\mathbf{r}), \tag{D34}$$

where $\tau_{1x}^{\mathrm{exp}}(\mathbf{r})$ and $\tau_{1y}^{\mathrm{exp}}(\mathbf{r})$ are given in eqs (D27) and (D28), respectively.